Neurobiology of Disease

Shift from Extracellular Signal-Regulated Kinase to AKT/cAMP Response Element-Binding Protein Pathway Increases Survival-Motor-Neuron Expression in Spinal-Muscular-Atrophy-Like Mice and Patient Cells

Julien Branchu,[1] Olivier Biondi,[1] Farah Chali,[1] Thibault Collin,[2] Felix Leroy,[3] Kamel Mamchaoui,[4] Joelle Makoukji,[1] Claude Pariset,[1] Philippe Lopes,[1,5] Charbel Massaad,[1] Christophe Chanoine,[1] and Frédéric Charbonnier[1]

[1]Centre d'Étude de la Sensorimotricité, Centre National de la Recherche Scientifique (CNRS) Unité Mixte de Recherche (UMR) 8194, [2]Laboratoire de Physiologie Cérébrale, CNRS UMR 8118, and [3]Neurophysique et Physiologie du Système Moteur, CNRS UMR 8119, Université Paris Descartes, Unité de Formation et de Recherche Biomédicale, F-75270 Paris, France, [4]Thérapie des Maladies du Muscle Strié/Institut de Myologie, Unité Mixte de Recherche en Santé 974 –Université Pierre et Marie Curie, Université Paris 6/Institut National de la Santé et de la Recherche Médicale Unité 974/CNRS UMR 7215, Groupe Hospitalier Pitié-Salpêtrière–Bâtiment Babinski, F-75651 Paris, France, and [5]Université d'Evry-val-d'Essonne, F-91000 Evry, France

Spinal muscular atrophy (SMA), a recessive neurodegenerative disease, is characterized by the selective loss of spinal motor neurons. No available therapy exists for SMA, which represents one of the leading genetic causes of death in childhood. SMA is caused by a mutation of the survival-of-motor-neuron 1 (*SMN1*) gene, leading to a quantitative defect in the survival-motor-neuron (SMN) protein expression. All patients retain one or more copies of the *SMN*2 gene, which modulates the disease severity by producing a small amount of stable SMN protein. We reported recently that NMDA receptor activation, directly in the spinal cord, significantly enhanced the transcription rate of the *SMN2* genes in a mouse model of very severe SMA (referred as type 1) by a mechanism that involved AKT/CREB pathway activation. Here, we provide the first compelling evidence for a competition between the MEK/ERK/Elk-1 and the phosphatidylinositol 3-kinase/AKT/CREB signaling pathways for *SMN2* gene regulation in the spinal cord of type 1 SMA-like mice. The inhibition of the MEK/ERK/Elk-1 pathway promotes the AKT/CREB pathway activation, leading to (1) an enhanced SMN expression in the spinal cord of SMA-like mice and in human SMA myotubes and (2) a 2.8-fold lifespan extension in SMA-like mice. Furthermore, we identified a crosstalk between ERK and AKT signaling pathways that involves the calcium-dependent modulation of CaMKII activity. Together, all these data open new perspectives to the therapeutic strategy for SMA patients.

Introduction

Spinal muscular atrophy (SMA), an autosomal recessive disease for which no therapy is presently available, is the leading genetic cause of death in childhood. SMA is characterized by a specific loss of spinal motor neurons, leading to a severe muscular weakness and irremediable death when vital muscles are affected (Crawford and Pardo, 1996). SMA can be classified into three types on the basis of the age of onset, time course, and range of motor-function loss. In the most severe type of SMA, referred to as type 1 or Werdnig–Hoffmann disease, which accounts for ~50% of patients diagnosed with SMA, the symptoms appear before 6 months of age, and death occurs in infancy or early childhood. SMA is caused by mutation of the survival-of-motor-neuron 1 (*SMN1*) gene (Lefebvre et al., 1995), leading to a deficiency of the survival-motor-neuron (SMN) protein expression. All patients retain one or more copies of the *SMN2* gene, which modulates the disease severity by allowing a small amount of full-length SMN transcripts and stable SMN protein to be produced (Lorson and Androphy, 2000).

Because SMA is caused by an insufficient amount of SMN protein, a major aim of SMA therapeutics strategy is to increase the levels of SMN protein generated by *SMN*2 gene expression. A number of groups have identified *SMN2* gene-inducing molecules (Chang et al., 2001; Avila et al., 2007; Thurmond et al., 2008; Tsai et al., 2008; Butchbach et al., 2010; Lorson et al., 2010), but so far, most of these agents yielded inconclusive results in clinical trials (Mercuri et al., 2007; Swoboda et al., 2009, 2010). An alternative promising therapeutic development for SMA, although as

Received June 7, 2012; revised Nov. 12, 2012; accepted Nov. 20, 2012.

Author contributions: J.B., O.B., C.M., and F.Char. designed research; J.B., O.B., F.Chal., T.C., F.L., K.M., and J.M. performed research; J.B., O.B., F.Chal., T.C., C.P., L.P., and C.C. analyzed data; J.B., O.B., C.P., L.P., and F.Char. wrote the paper.

This project was supported by the Association Française contre les Myopathies. J.B. is the recipients of a fellowship from the Ministry of Research and Technology, and F.Chal. is the recipient of a fellowship from AXA Research Fund/Garches Foundation. We thank G. Sanchez and J. Côté for help in molecular analysis, V. Mouly and the human cell culture platform of the Myology Institute (Paris, France) for the human cells from SMA patients, S. Lefebvre for antibodies, and Claire Mader for animal care.

Correspondence should be addressed to Frédéric Charbonnier, Université Paris Descartes, Unité de Formation et de Recherche Biomédicale, Centre d'Étude de la Sensorimotricité, Centre National de la Recherche Scientifique Unité Mixte de Recherche 8194, 45 rue des Saints-Pères, F-75270 Paris, France. E-mail: frederic.charbonnier@parisdescartes.fr.

DOI:10.1523/JNEUROSCI.2728-12.2013

 0270-6474/13/334280-15$15.00/0

yet unexplored, could be based on the pharmacological correction of molecular mechanisms that are altered in the SMA neuromuscular system, such as the AKT/CREB and ERK signaling pathways (Biondi et al., 2010). In striking contrast to AKT, the kinase ERK was found to be constitutively overactivated in mouse SMA spinal cord (Biondi et al., 2010). These observations raise important questions about the potential role of the ERK pathway in the regulation of *SMN2* gene expression that can be investigated in type 1 SMA-like mice spinal cord.

In the present study, using myotube cultures from type 2 SMA patients and type 1 SMA-like mice, we provide the first lines of evidence indicating that (1) the mitogen-activated protein kinase (MAPK) kinase (MEK)/ERK/Elk-1 pathway plays a repressive role on *SMN2* gene expression in SMA spinal cord, and (2) the pharmacological inhibition of the MEK/ERK/Elk-1 pathway resulted in an efficient AKT/CREB pathway activation through a calcium-dependent activation of CaMKII, finally leading to the increase of SMN expression and a significant neuroprotection. Importantly, the treatment of type 1 SMA-like mice by Selumetinib, which is currently in Phase II clinical trials (Board et al., 2009), induced a significant increase in SMA-like mouse lifespan, thus opening a new and promising way for treating the most severe types of this devastating disease.

Materials and Methods

Mice and treatments. The knock-out transgenic SMA-like mice [$Tg(SMN2)^{tg/tg}$;$Smn^{-/-}$ mice] were purchased from The Jackson Laboratory and genotyped as described previously (Monani et al., 2000). To standardize the type 1 SMA phenotype, male and female SMA-like mice phenotypically distinguishable from littermates at birth (as described by Monani et al., 2000) were used for this study. The SMA-like mice that displayed the first symptoms after 48 h of age were excluded from this study (<10% of SMA-like mice). This selection process allowed treatments to take place solely in the symptomatic phase of the disease. The selected SMA-like mice were slightly smaller (average weight, 1.08 ± 0.7 g) compared with heterozygous littermates (average weight, 1.52 ± 0.14 g). Vehicle-treated group, U0126 [1,4-diamino-2,3-dicyano-1,4-bis(o-aminophenylmercapto) butadiene]-treated group, and AZD6244 [5-(4-bromo-2-chloroanilino)-7-fluoro-*N*-(2-hydroxyethoxy)-3-methylbenzimidazole-5-carboxamide]-treated group of type 1 SMA-like mice were randomly constituted, regardless of weight or motor behavior to minimize bias. The control mice were heterozygous knock-out for *Smn* with the human *SMN2* transgene.

To evaluate the benefits of phospho-ERK inhibition, P1 neonate control and type 1 SMA-like mice were injected daily until P2, P6, or death intrathecally with 1 mg/kg U0126 (Sigma) in Evans Blue dyed 0.9% NaCl and 1% DMSO. Awake, conscious mice with intact muscle tone and reactions were injected at a 70–80% angle to the horizontal in the column maintained slightly curved to open up the intervertebral spaces. The injection was done over the course of 1–2 s. Mice were also treated orally with 5 mg/kg Selumetinib (AZD6244; Selleck Chemicals) in 0.9% NaCl and 1% DMSO. This treatment has been performed daily according to the pharmacokinetic and pharmacodynamics characteristics of AZD6244 in mice (Denton and Gustafson, 2011). For gavage, the head of the mice was maintained aligned with the esophagus, and a small rubber cannula was gently inserted 0.5 cm down the esophagus behind the incisors and directed toward the back of the throat. The injection course should not exceed 1–2 s to avoid cyanosis of the mouse's mucous membranes.

The treated-mice were compared with control and SMA-like mice either injected from P1 with 0.5 μl/g Evans Blue dyed 0.9% NaCl and 1% DMSO or orally treated with 2 μl/g 0.9% NaCl and 1% DMSO. The lifespan of 0.9% NaCl and 1% DMSO-treated mice (1.66 ± 0.55 d) proved to be similar to 0.9% NaCl-treated mice (1.65 ± 0.62 d; Biondi et al., 2010). Body weight and lifespan recordings were performed every day until the death of the animal. The animals were considered dead when mice were no longer able to stand up 1 min after having been placed on their sides.

The care and treatment of animals followed the national authority (French Ministry of Research and Technology) guidelines for the detention, use, and the ethical treatment of laboratory animals.

Behavioral evaluation. The time taken by mice to get back on their feet, after having been placed on the right side, was recorded in vehicle- and U0126-treated control and SMA-like mice from birth to P9 or death. Each mouse was subjected to five successive attempts separated by a 5 min rest period.

The ambulatory behavior was assessed in an open-field test for vehicle- and U0126-treated control and SMA-like mice. The apparatus consisted of a plastic box measuring 12 × 12 × 5 cm. The floor of the arena was divided into 16 3 × 3 cm squares. The mice were tested individually, and the open field was washed after each session. Each mouse initially placed in the center of the open field was allowed to move freely for 5 min. The behavioral measures recorded manually by the experimenter during these 5 min were the total number of square crossings and the mobility time.

Mouse cell cultures and treatments. Cocultures of mouse spinal cord explants (~1 mm^3) and muscle cells were performed as described by Kobayashi et al. (1987) for rat with the following modifications. Spinal cord explants were obtained from control and severe SMA-like embryonic mice. Explants from the whole transverse slices of 10.5-d-old mice embryo spinal cords including dorsal root ganglia (DRG) were placed on the muscle monolayer. DRG are essential to ensure a good innervation ratio (Kobayashi et al., 1987). The muscle culture was established through the differentiation of the wild-type muscle cell line C2C12. Myoblast cells were cultured on 35 mm Petri dishes at 37°C in 5% CO_2 in DMEM supplemented with 2 mM glutamine, 20% fetal bovine serum, and 2% penicillin/streptomycin (5000 U). All the culture medium reagents were purchased from Invitrogen. Confluent myoblasts were differentiated into myotubes in DMEM supplemented with 2 mM glutamine, 5% horse serum, and 2% penicillin/streptomycin (5000 U) [differentiation medium (DM)]. After 5–7 d in DM, spinal cord explants were added on the cultured contracting muscle cells. After coculture with spinal cord, the culture was kept in DM. All cocultures were fed three times a week and examined daily under a phase-contrast inverted microscope to follow the appearance of the innervation.

To evaluate the Ca^{2+} dependency, extracellular Ca^{2+} chelator EGTA (5 μM) (Sigma) and cell-permeable Ca^{2+} chelator BAPTA-AM (10 μM) (Invitrogen) was added to the culture. The role of the key signaling enzyme CaMKII was achieved by the treatment of cocultures by the inhibitor KN-93 (2-[*N*-(2-hydroxyethyl)]-*N*-(4-methoxybenzenesulfonyl)amino-*N*-(4-chlorocinnamyl)-*N*-methylbenzylamine) (10 μM) (Calbiochem).

Stimulation of the NMDA receptors was achieved by exposing cells to 100 μM NMDA, as described previously (Biondi et al., 2010). To evaluate the CREB dependency, KG-501 (3-[(4-chlorophenyl)carbamoyl]-2-naphthyl dihydrogen phosphate) (10 μM; Sigma) was added to the culture. After 5 d of treatment, explants were mechanically removed from the muscle layer, and proteins were purified and analyzed by Western blot as described below.

Human primary culture of myogenic precursor cells from SMA patient biopsies. Muscle biopsies were obtained from the Bank of Tissues for Research (a partner in the European Union network EuroBioBank) in accordance with European recommendations and French legislation. Satellite cells were isolated from biopsies and cultivated as described previously (Bigot et al., 2009) in growth medium consisting of 1 vol of 199 medium/4 vol of DMEM (Invitrogen) supplemented with 20% fetal calf serum (Invitrogen), 2.5 ng/ml hepatocyte growth factor (HGF) (Invitrogen), and 50 μg/ml gentamycin (Invitrogen). Because gentamycin can enhance SMN expression by itself (Heier and DiDonato, 2009), the same medium was dispatched in treated or untreated culture to ensure the same exposure to the drug. Additional expansion was made in growth medium without HGF. The myogenic purity of the populations was monitored by immunocytochemistry using desmin as a marker. Differentiation was induced at confluence by replacing the growth medium with DMEM supplemented with 4% horse serum and 50 μg/ml gentamycin (Sigma). Blockade of MEK phosphorylation was achieved using 10 μM U0126 (Sigma), 20 min/d, during 5 d.

Slice preparation. Control and SMA-like mice at 2 d of age were anesthetized with an intraperitoneal injection of 0.1 ml of pentobarbitol (20 mM). An intracardiac perfusion was performed using ice-cold low-Na^+ Ringer's solution containing the following (in mM): 3 KCl, 1.25 NaH_2PO_4, 230 sucrose, 26 $NaHCO_3$, 0.8 $CaCl_2$, 8 $MgCl_2$, 25 glucose, 0.4 ascorbic acid, and 1 kynurenic acid (bubbled with 95% O_2 and 5% CO_2), pH 7.4. After decapitation, the laminectomy was performed at 4°C in the same solution. After sectioning the roots, the spinal cord was transferred into a 2% agar solution at 38°C. Then, the solution was cooled to 4°C, and the agar block containing the spinal cord was cut and glued in the chamber of a slicer (Leica S100V). The slices were 300 μm thick. The slices were transferred into Ringer's solution at 34°C for 30 min and then brought to room temperature.

Calcium imaging. Motor neurons were identified using an upright microscope (Axioscop; Carl Zeiss) with Nomarski differential interference contrast optics, a 60× Olympus objective, 0.90 numerical aperture (NA) water-immersion objective, and a 0.63 NA condenser. Motor neurons were maintained under voltage clamp in the whole-cell recording (WCR) configuration at a holding potential of −70 mV. The intracellular solution contained the following (in mM): 140 K-gluconate, 5.4 KCl, 4.1 $MgCl_2$, 9.9 HEPES-K, 0.36 Na-GTP, 4 Na-ATP, and 0.1 Oregon Green 488 BAPTA-1 (Invitrogen). Tight-seal WCRs were obtained with borosilicate pipettes (4–6 MΩ) from superficial somata using an EPC-9 amplifier (HEKA). Series resistance values ranged from 15 to 25 MΩ and were compensated for by 60%. Currents were filtered at 1.3 kHz and sampled at a rate of 250 μs/point. Digital fluorescence images were obtained using an excitation-acquisition system from T.I.L.L. Photonics. Briefly, to excite fluorescence of the Ca^{2+} dye Oregon Green 488 BAPTA-1, light from a 75 W xenon lamp was focused on a scanning monochromator set at 488 nm and coupled, by a quartz fiber and a lens, to the microscope, equipped with a dichroic mirror and a high-pass emission filter centered at 505 and 507 nm, respectively. Images were acquired by a Peltier-cooled CCD camera (IMAGO QE; 1376 × 1040 pixels; pixel size, 244 nm after 63× magnification and 2 × 2 binning).

Histological and immunohistochemical analyses. Spinal cords were dissected and incubated overnight in 4% PFA PBS solution and washed twice for 2 h with PBS. The lumbar spinal cords (L1–L5) were embedded in 4% agarose solution in sterile water for 30 min at 4°C. Fifty-micrometer sections were then performed using a vibratome on the whole length of the sample. One of every five sections was processed for immunohistochemical analysis. Tissue sections were incubated for 1 h at room temperature in a blocking solution [10% normal donkey serum with 1% Triton X-100 and 0.5% Tween 20 in Tris-buffered saline (TBS)]. Motor neuron and Gemini of coiled bodies immunodetection were performed using a polyclonal goat anti-choline acetyltransferase (ChAT) primary antibody (1:400; Millipore Bioscience Research Reagents) and a monoclonal mouse anti-SMN primary antibody (1:200; BD Transduction Laboratories) for 4 d at 4°C in 3.5% donkey serum with 0.1% Tween 20 in TBS. Sections were washed between each subsequent step with 0.1% Tween 20 in TBS. Sections were subsequently incubated with polyclonal Cy3-conjugated donkey anti-goat antibodies (1:400; Jackson ImmunoResearch) and polyclonal Cy2-conjugated donkey anti-mouse antibodies (1:400; Jackson ImmunoResearch) for 1 h at room temperature in 3.5% donkey serum with 0.1% Tween 20 in TBS. The sections were washed three times for 10 min in 0.1% Tween 20 in TBS and mounted in Fluoromount G (Southern Biotechnology) mounting medium. The staining specificity was checked in control incubations performed in the absence of the primary antibody.

All counts were performed using NIH ImageJ software version 1.37. Color images were tinted using Image Pro-Plus software, in which identical brightness, contrast, and color balance adjustments were applied to all groups.

Microscopy. All immunofluorescence images were collected with a CCD camera (QImaging Retiga 2000R Fast, Cooled Mono 12 bit) mounted on Olympus microscope (BX51) using the Image Pro-Plus version 6.0 software (MediaCybernetics) with 40× (4× Olympus objective UPlan FL N 0.13), 100× (10× Olympus objective UPlan FL N 0.3), 200× (20× Olympus objective FL N 0.5), 400× (40× Olympus objective UPlan FL N 0.75), 600× (60× Olympus objective UPlanS Apo 1.35 oil), and 1000× (100× Olympus objective UPlanS Apo 1.4 oil) magnifications.

Protein and Western blot analyses. The ventral part of frozen spinal cord was separated from the dorsal part by razor blade at −20°C. The dissection is performed at the level of the depression that separates the ventral from the dorsal part of the spinal cord. Brain, heart, kidneys, lungs, liver, diaphragm, tibialis muscle, and ventral lumbar spinal cord samples (2–5 mg) were homogenized in 100 μl/5 mg tissues in the presence of ice-cold RIPA buffer [50 mM Tris HCl, pH 8.0, 150 mM NaCl, 0.1% SDS, 0.5% sodium deoxycholate, 1% NP-40, 5 mM EDTA, pH 8.0, 2 mM PMSF (Sigma-Aldrich), 50 μg/ml leupeptin, 50 μg/ml pepstatin A, and 50 μg/ml aprotinin]. Protein concentration of the clarified homogenates (4°C, 15 min, 13,500 rpm) was determined on all samples using the Bradford protein assay (Bio-Rad). Ten-microgram protein samples for SMN analysis and 30 μg samples for other analysis of each homogenate were submitted to 12.5% SDS-PAGE electrophoresis (1.5 M Tris, pH 8.3, 12.5% acrylamide, 0.07% Bis, 0.1% SDS, 0.05% ammonium persulfate, and 0.06% N,N,N',N'-tetramethylethylene diamine). The separated proteins were transferred on PVDF membranes (Bio-Rad) (Towbin et al., 1984). Equal loading of samples was checked by Ponceau dye staining of the transferred gels. Western blot analysis was performed on membranes incubated overnight at 4°C in 4% BSA, 0.1% Tween 20, and TBS, pH 7.4. Each of the following primary antibodies, including monoclonal mouse anti-SMN (1:5000; Santa Cruz Biotechnology), polyclonal rabbit anti-Thr305 phospho-CaMKII (1:1000; Millipore Bioscience Research Reagents), polyclonal rabbit anti-Ser473 phospho-AKT (1:1000; Cell Signaling Technology), polyclonal rabbit anti-phospho-ERK1/2 (1:500; Cell Signaling Technology), polyclonal rabbit anti-Ser133 phospho-CREB (1:1000; Millipore), monoclonal mouse anti-Ser183 phospho-Elk-1 (1:1000; Santa Cruz Biotechnology) was incubated overnight at 4°C in the above blocking medium. Membranes were rinsed in 0.1% Tween 20 in TBS for three times for 10 min at room temperature and then incubated in horseradish peroxidase-conjugated goat secondary antibody directed against mouse Igs (1:5000; Bio-Rad) and in horseradish peroxidase-conjugated goat secondary antibody directed against rabbit Igs (1:10,000; Jackson ImmunoResearch) in 0.1% Tween 20 in TBS for 1 h at room temperature. Bound antibody complexes were developed using the ECL system (GE Healthcare) and exposed to hyperfilm ECL-plus x-ray film (GE Healthcare).

In some instances, membranes were stripped after immunoblotting with phospho-CaMKII, phospho-AKT, phospho-ERK1/2, phospho-CREB, and phospho-Elk-1 by incubation in stripping buffer (100 mM β-mercaptoethanol, 2% SDS, and 62.5 mM Tris-HCl, pH 6.7) for 30 min at 55°C with agitation, and membranes were then blocked and reprobed with polyclonal rabbit anti-CaMKII (1:1000; Santa Cruz Biotechnology), polyclonal rabbit anti-AKT (1:1000; Cell Signaling Technology), polyclonal rabbit anti-ERK1/2 (1:500; Cell Signaling Technology), polyclonal rabbit anti-CREB (1:1000; Millipore), monoclonal mouse anti-Elk-1 (1:1000; Santa Cruz Biotechnology), and monoclonal mouse anti-glyceraldehyde-3-phosphate dehydrogenase antibody (GAPDH) (1:5000; Millipore Bioscience Research Reagents). Films were quantified with NIH ImageJ version 1.37, and the results reported as means ± SEM.

Chromatin immunoprecipitation. Ventral lumbar spinal cord samples were chopped into small pieces with a scalpel and were fixed for 15 min with 1% formaldehyde. Tissues were washed three times in cold PBS containing protease inhibitors (2 mM PMSF, 50 μg/ml leupeptin, 50 μg/ml pepstatin A, and 50 μg/ml aprotinin) and collected by centrifugation. Cells were pelleted by centrifugation and resuspended in 300 μl of 85 mM KCl, 0.5% NP-40, and 5 mM piperazine-*N*,*N*′-bis(2-ethanosulfonic acid), pH 8.0, in the presence of protease inhibitors (2 mM PMSF, 50 μg/ml leupeptin, 50 μg/ml pepstatin A, and 50 μg/ml aprotinin). After incubation on ice for 10 min, cells were sonicated six times for 30 s using Bioruptor (Diagenode). Lysates were cleared by centrifugation, and DNA concentration was determined by nanodrop spectrophotometer. ChIP-Adembeads (Ademtech) were incubated for 15 min at room temperature with blocking buffer on a rotating wheel. Beads were resuspended in 125 μl of chromatin immunoprecipitation (ChIP) dilution buffer (0.01% SDS, 1% Triton X-100, 1.2 mM EDTA, and 16.7 mM Tris-HCl, pH 8.1), and after a 1 h incubation, equal amounts of DNA diluted 10 times in dilution buffer were added. DNA was incubated over-

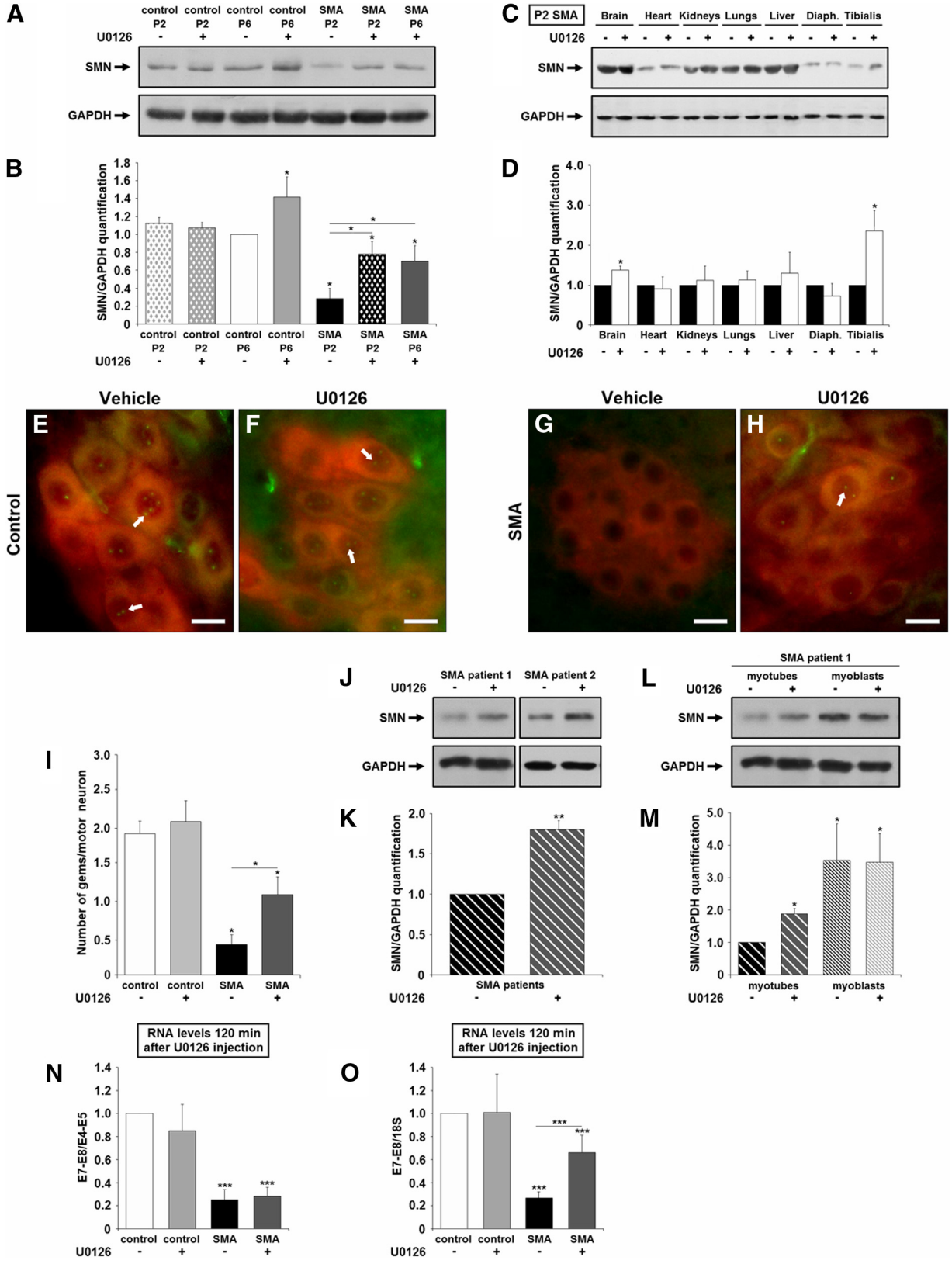

Figure 1. ERK pathway inhibition by U0126 induces a significant increase in SMN expression in the motor neurons of severe SMA-like mice and in myogenic cells of severe-type SMA patients. ***A***, ***B***, Western blot analysis and quantification of SMN protein expression in the ventral lumbar spinal cord of vehicle- and U0126-treated control mice at 2 and 6 d of age, vehicle-treated SMA-like mice at 2 d of age, and U0126-treated SMA-like mice at 2 and 6 d of age ($n = 3$). ***C***, ***D***, Western blot analysis and quantification of SMN protein expression in brain, heart, kidneys, lungs, liver, diaphragm, and tibialis of U0126-treated SMA-like mice at 2 d of age ($n = 3$). ***E–I***, Immunodetection of gems in ChAT-positive motor neurons in the lumbar spinal cord (L1–L5) of vehicle-treated (***E***) and U0126-treated control (***F***) mice at 6 d of age, vehicle-treated SMA-like mice at 2 d of age (***G***), and U0126-treated SMA-like mice at 6 d of age (***H***). Scale bar, 25 μm. Quantitative analysis of gems per motor neuron (***I***). ***J***, ***K***, Western blot analysis and quantification of SMN protein expression in vehicle- and U0126-treated human SMA cultured myotubes from two type 2 SMA patients ($n = 3$ each patient). ***L***, ***M***, Western blot analysis and quantification of SMN protein expression in vehicle- and U0126-treated human SMA cultured myotubes and myoblasts from a (*Figure legend continues.*)

night at 4°C on a rotating wheel with 1 μg of the following antibodies: polyclonal rabbit anti-Ser133 phospho-CREB (Millipore), monoclonal mouse anti-Ser183 phospho-Elk-1 (Santa Cruz Biotechnology), polyclonal rabbit anti-acetyl-histone H3 Lys9 (Millipore), and polyclonal rabbit-acetyl-histone H4 Lys8 (Millipore). Beads were washed sequentially in 150 mM NaCl TSE [0.1% SDS, 1% Triton X-100, 2 mM EDTA, 20 mM Tris-HCl, pH 8.1, with 500 mM NaCl TSE, buffer A (0.25 M LiCl, 1% NP-40, 1% deoxycholate, 1 mM EDTA, and 10 mM Tris-HCl, pH 8.1)] and two times with Tris-EDTA, pH 8.1, and then selectively eluted with 200 μl of 1% SDS and 0.1 M $NaHCO_3$. Crosslinks were reversed by heating at 65°C for 4 h after adding NaCl at a 200 mM final concentration. After treatment with proteinase K (50 μg/ml) for 1 h at 37°C, DNA was purified using Geneclean Turbo Kit (Q-Biogene; MP Biomedicals). Real-time PCR analysis of inputs or immunoprecipitated DNAs was performed.

Quantitative real-time PCR analysis. Ventral lumbar spinal cord samples were chopped into small pieces with a scalpel, and RNA was extracted using Trizol (Invitrogen). Each RNA preparation was treated with RQ1 RNase-Free DNase (Promega). One microgram was reverse transcribed with random primers (Promega) and reverse transcriptase MMLV-RT (Invitrogen).

Quantitative real-time PCR was performed with standard protocols using SYBRGreen ROX Mix (ABgene) as a fluorescent detection dye in ABI PRISM 7000 in a final volume of 10 μl, which also contains 300 nM of the following primers (Operon): SMN2 exon 4–exon 5 segment forward, 5′-TGTGTTGTGGTTTACACTGG-3′; SMN2 exon 4–exon 5 segment reverse, 5′-TATTTCCAGGAGACCTGGAG-3′; SMN2 exon 7–exon 8 segment forward, 5′-AAAAAGAAGGAAGGTGCTCAC-3′; SMN2 exon 7–exon 8 segment reverse, 5′-GCCTCACCACCGTGCTGG-3′; 18S forward, 5′-GTAACCCGTTGAACCCCATT-3′; 18S reverse, 5′-CCATCCAATCGGTAGTAGCG-3′; SMN2 promoter site 1 [−2667nu to −2401nu] forward, 5′-GAGAGAGTTCCAGGAGTCAA-3′; SMN2 promoter site 1 [−2667nu to −2401nu] reverse, 5′-GTCTCAAACTCGGTTGCTT-3′; SMN2 promoter site 2 [+160nu to +503nu] forward, 5′-TCGTAGAAAGCGTGAGAAGT-3′; and SMN2 promoter site 2 [+160nu to +503nu] reverse, 5′-AAAACGCGGACCACAACTC-3′. The relative amounts of DNA in samples were determined on the basis of the threshold cycle for each PCR product.

Statistical analyses. All values are displayed as means ± SEM within each group (Systat version 8.0; SPSS). Statistical analysis was performed and comparison between groups were done using ANOVA and *post hoc* test least significant difference test. Survival analysis was performed using Kaplan–Meier analysis.

Results

The inhibition of the MEK/ERK/Elk-1 pathway by U0126 promoted SMN expression in the spinal cord of type 1 SMA-like mice and in myotubes of severe-type SMA patients

Sustained activation of ERK1/2 correlated with low SMN expression level in SMA spinal cord (Biondi et al., 2010). To test the assumption of a causal link between the ERK pathway activation and the SMN expression levels, we analyzed the effects of ERK *in vivo* inhibition in SMA spinal cord. For this purpose, a population of type 1 SMA-like mice was treated daily from birth by intrathecal injection of U0126 (1 $mg \cdot kg^{-1} \cdot d^{-1}$), an MEK inhibitor leading to ERK inhibition. We found that this *in vivo* ERK inhibition resulted in a significant increase in SMN protein concentration in the spinal cord of type 1 SMA-like mice (Fig. 1*A*,*B*). The U0126-induced increase of SMN expression proved to be tissue dependent (Fig. 1*C*,*D*). The SMN level remained constant during the treatment period. These data are further substantiated by the significant increase of Gemini of coiled bodies (gems) in the motor neuron nuclei of U0126-treated SMA-like mice (Fig. 1*E–I*).

Consistent with our findings in SMA-like mice, the inhibition of the ERK pathway by U0126 in myotube culture of paravertebral muscles from type 2 SMA patients resulted in a significant SMN expression increase (Fig. 1*J*,*K*). To determine whether these effects of ERK inhibition occurred at all stages of muscle differentiation, we analyzed SMN expression in myoblasts (Fig. 1*L*,*M*). No ERK inhibition-induced effect was apparent in myoblasts, suggesting that the positive regulatory effect of ERK inhibition on AKT and SMN is restricted to differentiated muscle cells, accounting for previous studies indicating differentiation stage-specific crosstalks between ERK and AKT in muscle cells (Rommel et al., 1999; Zimmermann and Moelling, 1999).

To determine whether the increased SMN protein level resulted from an activation of *SMN2* gene expression and/or from a modulation of the exon 7 insertion in the SMN transcripts, we quantified the fraction of exon 7-containing mRNA inside the population of SMN transcripts using real-time RT-PCR aimed at amplifying either the exon 7–exon 8 segment or the exon 4–exon 5 segment in the lumbar spinal cord of vehicle- and U0126-treated control and SMA-like mice at 2 d of age (Fig. 1*N*,*O*). Expectedly, SMA-like mice showed a dramatic reduction (>74% reduction) in exon 7-containing SMN transcripts compared with control mice. As early as 2 h after U0126 treatment, a significant 2.5-fold increase in *SMN2* gene expression in the SMA-like mice was recorded. The inclusion profile of exon 7 in SMN transcripts kept unmodified, suggesting that this ERK-mediated inhibitory effect occurred at the transcriptional level. This global activation of *SMN2* gene transcription led to an increase from 26 to 65% of exon 7-containing SMN transcripts in U0126-treated SMA spinal cord. In addition, the 2 h delay between the U0126 treatment and the *SMN2* gene transcriptional activation suggested that the ERK inhibition effects occurred directly, without any additional transcription event.

The MEK/ERK/Elk-1 and the PI3K/AKT/CREB signaling pathways are in competition for SMN2 gene regulation in the spinal cord of type 1 SMA-like mice

Because these data suggested for the first time that the ERK pathway might have a crucial role in the regulation of SMN expression, we analyzed the effects of ERK inhibition at the level of *SMN* gene promoter. Interestingly, when we analyzed the sequence of the human *SMN* promoter (GenBank accession number AF187725), we found that several CREB binding sites were flanked by putative response elements for Elk-1, a transcription factor of the ETS family, known to be a direct target of ERK (Whitmarsh et al., 1995; Yang et al., 1999; Zhang et al., 2008). These sites include response elements for Elk-1 itself or for the Elk-1-containing serum response factor (SRF). More precisely, the CREB binding site 2 (+244 to +248 bp), considered as a positive regulator of SMN gene expression (Majumder et al., 2004), is flanked by putative response elements for Elk-1 and SRF (+356 to +429 bp) (Fig. 2*B*). We identified an additional putative CRE site (referred to as site 1) that includes two potential CREB binding sites (−2572 to −2569 bp and −2525 to −2522 bp) and also two potential SRF binding sites (−2556 to −2548 bp) (Fig. 2*A*). We performed ChIP experiments aimed at evaluating the respective binding of CREB and Elk-1 to these two sites. We have initially analyzed the activation profile of the two transcription factors, namely Elk-1 and CREB, in the spi-

←

(*Figure legend continued.*) type 2 SMA patient ($n = 3$). ***N***, ***O***, Quantification by real-time RT-PCR of exon 7–exon 8 (E7-E8) segment containing SMN transcripts normalized either by exon 4–exon 5 (E4-E5) segment containing SMN transcripts (***N***) or by 18S transcripts (***O***) in the ventral lumbar spinal cord of vehicle- and U0126-treated control and SMA-like mice at 2 d of age ($n = 9$). Data are displayed as mean ± SEM. $^{*}p < 0.05$, $^{**}p < 0.01$, $^{***}p < 0.001$.

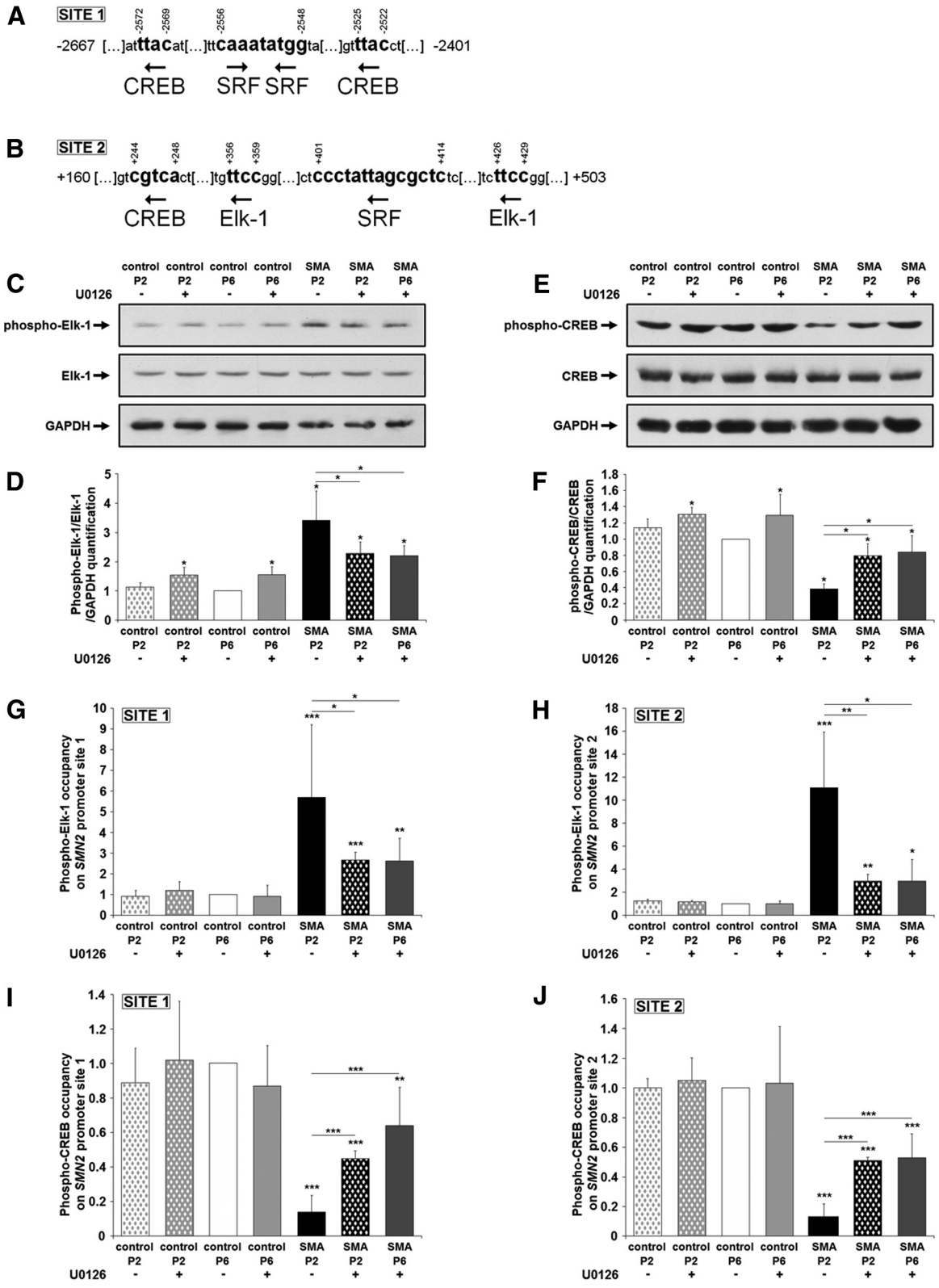

Figure 2. Activated Elk-1 and CREB transcription factors compete for binding the *SMN2* promoter in the spinal cord of severe SMA-like mice. ***A***, ***B***, SMN promoter site 1 (***A***) and site 2 (***B***) sequences. ***C–F***, Western blot analysis and quantification of Elk-1 protein (***C***, ***D***) phosphorylation and CREB protein (***E***, ***F***) phosphorylation in the ventral lumbar spinal cord of vehicle- and U0126-treated control mice at 2 and 6 d of age, vehicle-treated SMA-like mice at 2 d of age, and U0126-treated SMA-like mice at 2 and 6 d of age ($n = 3$). ***G–J***, ChIP analysis of phospho-Elk-1 (***G***, ***H***) and phospho-CREB (***I***, ***J***) in the ventral lumbar spinal cord of vehicle- and U0126-treated control mice at 2 and 6 d of age, vehicle-treated SMA-like mice at 2 d of age, and U0126-treated SMA-like mice at 2 and 6 d of age ($n = 9$). Quantitative real-time PCR was performed to detect SMN2 promoter site 1 (***G***, ***I***) and site 2 (***H***, ***J***). Data are displayed as mean ± SEM. $*p < 0.05$, $**p < 0.01$, $***p < 0.001$.

nal cord of vehicle- and U0126-treated type 1 SMA-like mice and controls. Elk-1 was found to be overactivated in the spinal cord of type 1 SMA-like mice (Fig. 2*C*,*D*), as expected for a direct target of ERK, contrasting with CREB downactivation (Fig. 2*E*,*F*). The U0126-treatment induced a marked increase in CREB activation in SMA spinal cord (Fig. 2*E*,*F*) and a parallel decrease of Elk-1 activation level only in SMA spinal cord (Fig. 2*C*,*D*). We found that the two transcription factors effectively bind the two Elk-1/CREB binding sites but with an efficiency that correlated with their activation levels. Elk-1 displayed an increased binding on the two sites in SMA spinal cord compared with controls (Fig. 2*G*,*H*). In contrast, ChIP experiments revealed a dramatic decrease in the binding of CREB on its two specific sites in SMA spinal cord (Fig. 2*I*,*J*). Interestingly, the CREB versus Elk-1 binding ratio to their respective sites was completely reversed in SMA spinal cords after ERK pathway inhibition by U0126 (Fig. 2*G–J*).

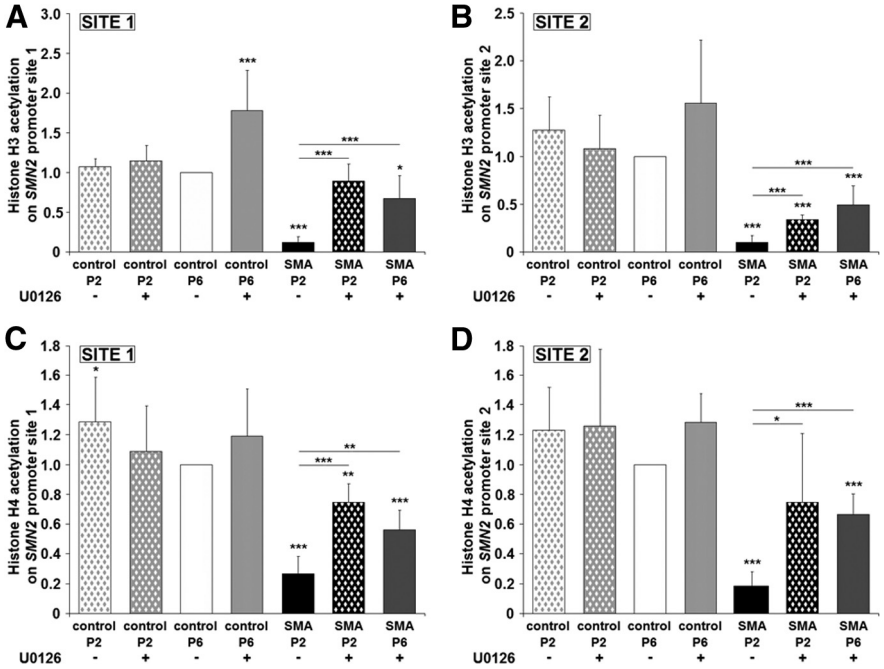

Figure 3. ERK pathway inhibition by U0126 alters H3 and H4 acetylation profiles in the spinal cord of severe SMA-like mice. ***A–D***, ChIP analysis of histone H3 (***A***, ***B***) and H4 (***C***, ***D***) acetylation in the ventral lumbar spinal cord of vehicle- and U0126-treated control mice at 2 and 6 d of age, vehicle-treated SMA-like mice at 2 d of age, and U0126-treated SMA-like mice at 2 and 6 d of age ($n = 9$). Quantitative real-time PCR was performed to detect SMN2 promoter site 1 (***A***, ***C***) and site 2 (***B***, ***D***). Data are displayed as mean ± SEM. $^{*}p < 0.05$, $^{**}p < 0.01$, $^{***}p < 0.001$.

We then questioned whether Elk-1 might play a repressive role on *SMN2* gene expression. We used ChIP analysis for the determination of histones H3 and H4 acetylation level on the two Elk-1/CREB binding sites in the spinal cord of SMA-like and control mice. Elk-1 recruitment to the two sites correlated to a marked decrease of H3 and H4 acetylation compared with controls, whereas CREB recruitment, after U0126 treatment, induced a marked increase of H3 and H4 acetylation (Fig. 3*A–D*). Together, these unexpected results suggest that the ERK/Elk-1 pathway activation results in the repression of *SMN2* gene expression in SMA spinal cord. Moreover, the ERK inhibition-induced activation of CREB in SMA spinal cord is likely to act synergistically with the Elk-1 inhibition, leading to an increased overall SMN gene expression.

CaMKII constitutes the molecular basis for ERK and AKT crosstalk in SMA spinal cord

The fact that ERK inhibition induced CREB activation prompted us to analyze the activation profile of AKT, which is considered as an efficient CREB activating kinase in SMA spinal cord (Biondi et al., 2010). We found that the ERK inhibition resulted in a significant activation of AKT in the spinal cord of SMA-like mice (Fig. 4*A*,*B*), as well as in human myotubes from SMA patients (Fig. 4*C*,*D*). An AKT-induced inhibition of ERK has been described previously (Majumder et al., 2004; Millino et al., 2009), yet a possible involvement of ERK activation level in the control of AKT activation was totally unexpected. Among the possible mechanisms involved in this new crosstalk, CaMKII represented an attractive candidate because (1) in all likelihood, it is situated upstream of ERK and AKT in the signaling cascades (Sutton and Chandler, 2002) and (2) its pattern of activation parallels AKT activation pattern in SMA spinal cord (Biondi et al., 2010). Thus, we have investigated whether the signal generated by ERK inhibition could result in the activation of CaMKII, AKT, and ultimately CREB. The *in vivo* inhibition of CaMKII in control and SMA spinal cord by KN-93 abolished the ERK-inhibition-induced activation of CREB (Fig. 4*E*,*F*). We next investigated the kinetics of CaMKII, AKT, and CREB activation after *in vivo* ERK inhibition in control and SMA-like mice (Fig. 4*G–N*). At 30 min after ERK inhibition, CaMKII and AKT were already activated, and the signal is transmitted to CREB 60 min after ERK inhibition. These data suggested that the crosstalk between ERK and AKT pathways was direct and independent of any additional transcription event. Together, all these data suggest that, at the intracellular level, the transduction signal could shift from a signaling pathway to the other by targeting of a common controlling kinase such as CaMKII, situated upstream of ERK and AKT.

The ERK inhibition induces a calcium flux in SMA spinal cord

We next questioned whether the ERK inhibition-induced activation of CaMKII was a consequence of an increased calcium influx. To directly address this question, we used an *in vitro* protocol, based on the coculture of spinal cord explants collected from type 1 SMA-like and control embryos (E10.5) grown on a monolayer of contractile muscle fibers, as described previously (Biondi et al., 2010). We first ascertained that the U0126 treatment of the cocultures induced a strong increase (twofold) in SMN protein expression in the SMA explants (Fig. 5*C*,*D*). The same effects were observed in control explants albeit to a lower magnitude (Fig. 5*A*,*B*). We then analyzed the effects of calcium influx blocking. Chelating extracellular Ca^{2+} by EGTA, or intracellular Ca^{2+} by the cell-permeable Ca^{2+} chelator BAPTA-AM, completely blocked the U0126-induced increase of SMN protein expression (Fig. 5*A–D*), CaMKII activation (Fig. 5*E–H*), and CREB activation (Fig. 5*I–L*) in control and SMA explants. Taken as a whole, these data suggest that the ERK inhibition-induced activation of CaMKII was calcium influx dependent.

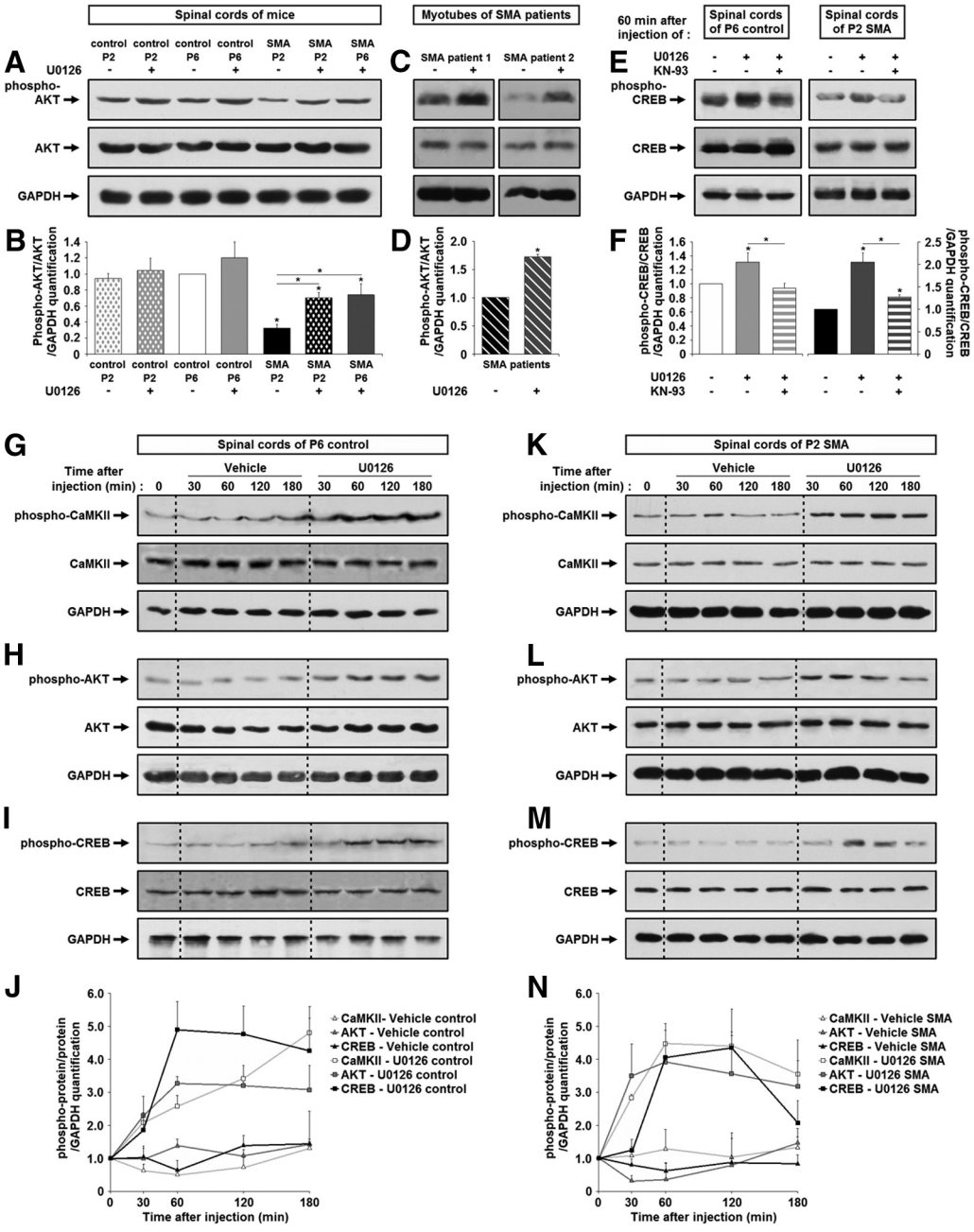

Figure 4. ERK pathway inhibition by U0126 leads to CaMKII activation and triggers the AKT/CREB pathway in the spinal cord of SMA-like mice. ***A–D***, Western blot analysis and quantification of AKT protein in the ventral lumbar spinal cord of vehicle- and U0126-treated control mice at 2 and 6 d of age, vehicle-treated SMA-like mice at 2 d of age, and U0126-treated SMA-like mice at 2 and 6 d of age (***A***, ***B***) ($n = 3$) and in vehicle- and U0126-treated human SMA cultured myotubes from two type 2 SMA patients (***C***, ***D***) ($n = 3$). ***E***, ***F***, Western blot analysis and quantification of CREB protein phosphorylation in the ventral lumbar spinal cord of control mice at 6 d of age and SMA-like mice at 2 d of age, treated by vehicle, ERK inhibitor U0126 with or without CaMKII inhibitor KN-93 ($n = 3$). ***G–J***, Kinetic analysis by Western blot of CaMKII protein activation (***G***), AKT protein activation (***H***), and CREB protein activation (***I***) after *in vivo* ERK inhibition by U0126 in spinal cords of control mice at 6 d of age and quantifications ($n = 2$) (***J***). ***K–N***, Kinetic analysis by Western blot of CaMKII protein activation (***K***), AKT protein activation (***L***), and CREB protein activation (***M***) after *in vivo* ERK inhibition by U0126 in spinal cords of SMA-like mice at 2 d of age and quantifications ($n = 2$) (***N***). Data are displayed as mean ± SEM. $^*p < 0.05$.

To get a closer insight into a direct involvement of Ca^{2+} in these ERK-inhibition-induced effects, neurons located in the ventral motor column of the lumbar spinal cord in control and SMA-like mice were loaded with the Ca^{2+} indicator Oregon Green 488 BAPTA-1 through the whole-cell configuration of the patch-clamp technique in living spinal cord sections. Ca^{2+} fluctuations were monitored 30 min after probe loading, whereas the Ca^{2+} fluorescence has reached a plateau. The cells were then submitted to U0126 for 45 min. Addition of U0126 (10 μM) to the incubation medium induced a net increase in the cytosolic ($\Delta F/F0 = 50.75 \pm 16.85\%$, $n = 4$) Ca^{2+} for both strains (exemplified on Fig. 5*M*). On the basis of their electrophysiological properties (i.e., capacitance superior to 30 pF and presence of spikes under the cell-attached configuration; see Fig. 5, inset), it can be concluded that the recorded cells are motor neurons. Together, these data suggest that ERK inhibition induced a raise in Ca^{2+} cytosolic concentration that originates from either a Ca^{2+} entry within the cell or a Ca^{2+} release from internal stores.

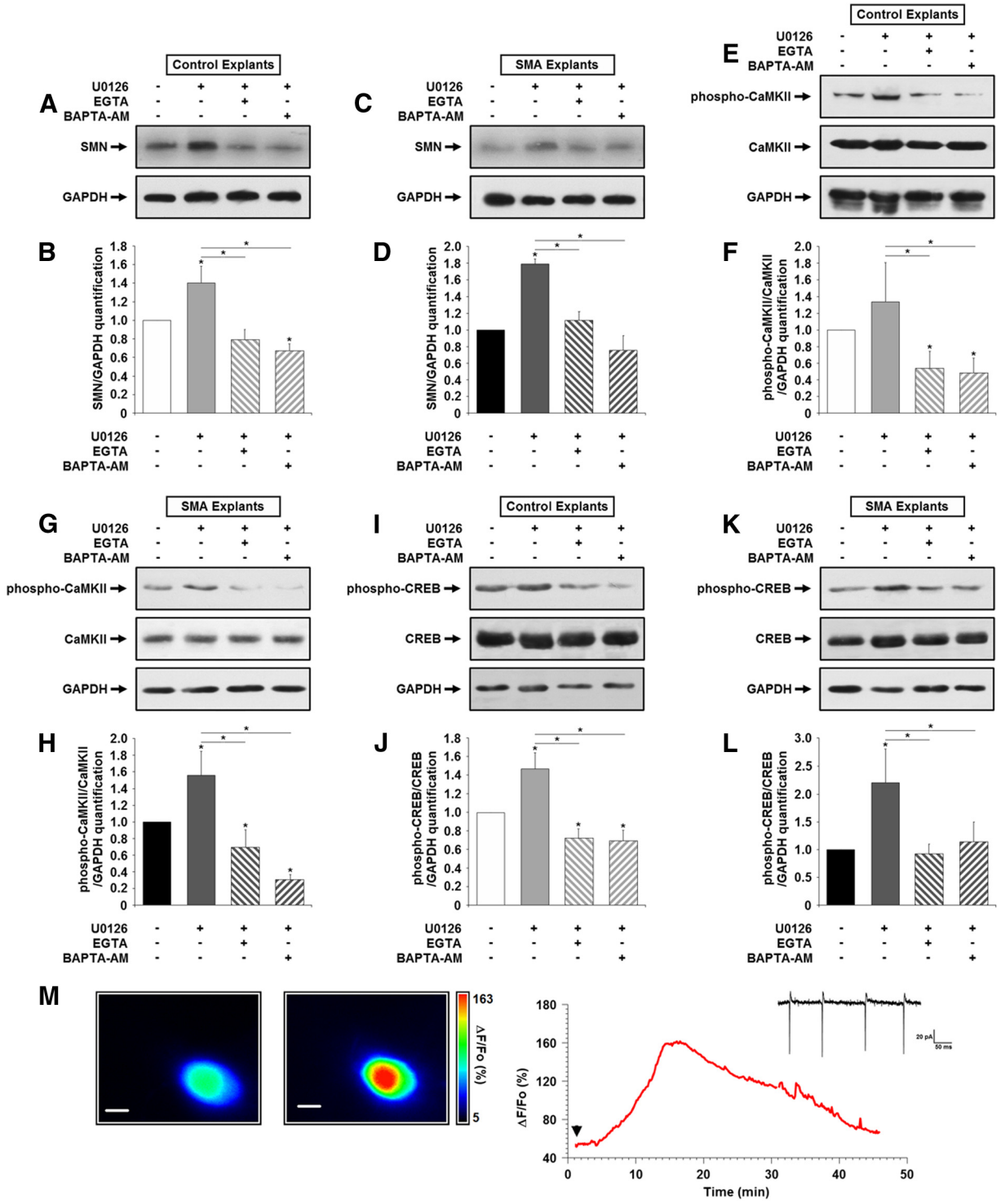

Figure 5. The alteration of intracellular pathways induced by ERK pathway inhibition is Ca^{2+} influx dependent. ***A–D***, Western blot analysis and quantification of SMN protein expression in control (***A***, ***B***) and SMA (***C***, ***D***) spinal cord explants in the presence or absence of U0126 or the calcium chelators EGTA and BAPTA-AM ($n = 3$). ***E–H***, Western blot analysis and quantification of CaMKII protein phosphorylation in control (***E***, ***F***) and SMA (***G***, ***H***) spinal cord explants in the presence or absence of U0126 or either the calcium chelators EGTA and BAPTA-AM ($n = 3$). ***I–L***, Western blot analysis and quantification of CREB protein phosphorylation in control (***I***, ***J***) and SMA (***K***, ***L***) spinal cord explants in the presence or absence of U0126 or either the calcium chelators EGTA and BAPTA-AM ($n = 3$). ***M***, Time course of the U0126 effect on an Oregon Green 488 BAPTA-1-loaded motor neurons recorded in spinal cord section of a control mouse. Images represent either the basal fluorescence level (left side) or the fluorescence at the peak of the response (right side). Scale bars, 20 μm. Inset shows spikes recorded on the same cell under the cell-attached configuration of the patch clamp. Data are displayed as mean ± SEM. *$p < 0.05$.

The AKT/ERK equilibrium is shifted by reciprocal blockades in SMA spinal cord

To investigate whether the crosstalk at the level of the ERK and AKT kinases are reciprocal, we tested in the cocultures the effects of CREB inhibition on the ERK/Elk-1 pathway activation profile in controls and in an SMA context in which the AKT pathway was significantly activated through the NMDA receptor activation. We found that CREB inhibition resulted in the activation of ERK

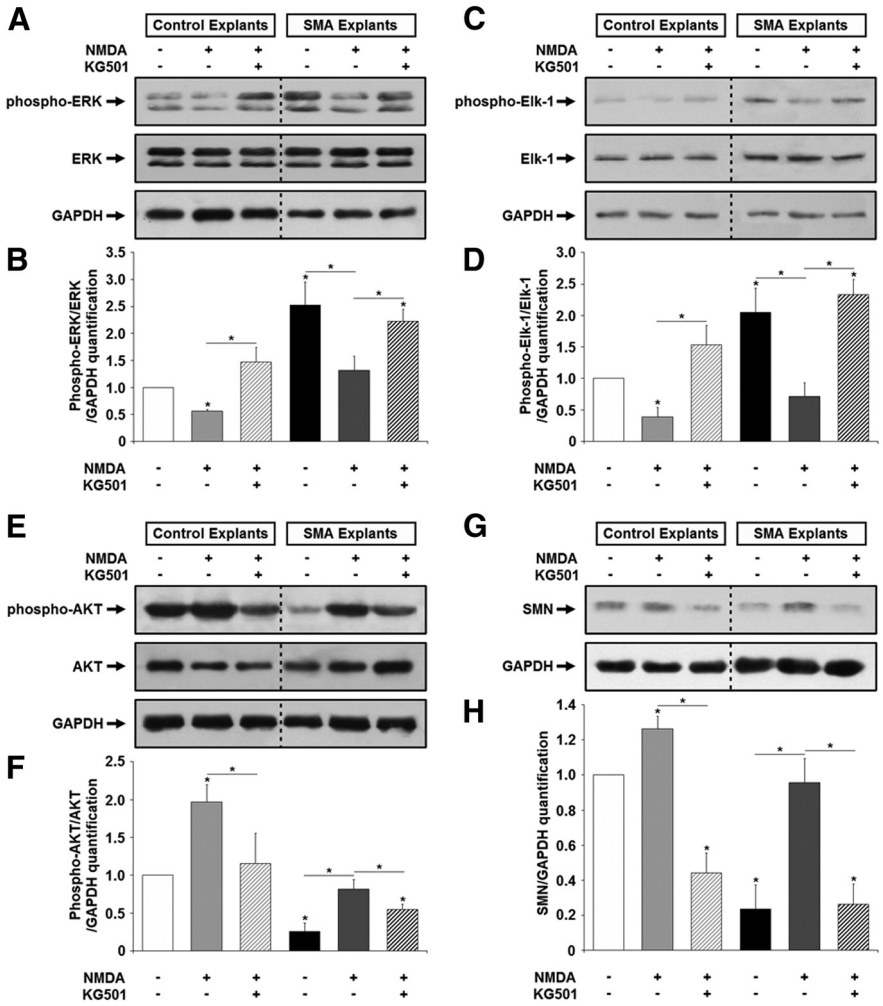

Figure 6. The crosstalk between ERK and AKT signaling pathways is reciprocal in SMA spinal cord. ***A***, ***B***, Western blot analysis and quantification of ERK protein phosphorylation in control and SMA spinal cord explants in the presence or absence of either NMDA or the CREB inhibitor KG-501 ($n = 3$). ***C***, ***D***, Western blot analysis and quantification of Elk-1 protein phosphorylation in control and SMA spinal cord explants in the presence or not of NMDA and of the CREB inhibitor KG-501 ($n = 3$). ***E***, ***F***, Western blot analysis and quantification of AKT protein phosphorylation in control and SMA spinal cord explants in the presence or absence of either NMDA or the CREB inhibitor KG-501 ($n = 3$). ***G***, ***H***, Western blot analysis and quantification of SMN protein expression in control and SMA spinal cord explants in the presence or absence of NMDA or the CREB inhibitor KG-501 ($n = 3$). Data are displayed as mean ± SEM. *$p < 0.05$.

(Fig. 6*A*,*B*) and Elk-1 (Fig. 6*C*,*D*) in close agreement with our hypothesis. More surprisingly, the CREB inhibition resulted in a significant inhibition of AKT (Fig. 6*E*,*F*), suggesting a negative feedback from the transcription factor to its activating kinase. This inhibition correlated to a significant decrease in SMN expression in control and SMA explants (Fig. 6*G*,*H*). Together, these data strongly suggest the existence of a dynamic equilibrium between ERK and AKT pathways in SMA spinal cord. This equilibrium could be shifted by reciprocal blockades, thus opening a promising way for reactivating the AKT/CREB-pathway-induced neuroprotection in impaired neurons.

The inhibition of the MEK/ERK/Elk-1 pathway by U0126 limits motor neuron loss and significantly extends the lifespan of type 1 SMA-like mice

Because the ERK inhibition is likely to activate SMN expression in SMA motor neurons, we questioned whether this effect could be beneficial in protecting motor neurons from cell death. To this end, we compared the number of ChAT-positive motor neurons in the ventral spinal cord of control mice and vehicle- or U0126-treated SMA-like mice (Fig. 7*A*–*G*). At 2 d of age, a 31.37% loss of motor neurons was observed in the vehicle-treated type 1 SMA-like mice compared with untreated P2 controls (Fig. 7*H*). In contrast, U0126-treated type 1 SMA-like mice only display 11.84% reduction in the number of motor neurons at 2 d of age. At 6 d of age, a 15.36% reduction was observed in U0126-treated SMA-like mice compared with controls, demonstrating that the ERK inhibition significantly limited the extent of motor neuron death ($p < 0.05$). Furthermore, motor neuron cell-body-area evaluation provided evidence for a persistent atrophy of motor neurons in the ventral horn of the spinal cord of the vehicle-treated type 1 SMA-like mice compared with control mice at 2 d of age (Fig. 7*I*). In contrast, the extent of atrophy is significantly limited in U0126-treated mice ($p < 0.05$) (Fig. 7*J*). No difference could be observed in the number of motor neurons in U0126- and vehicle-treated control mice at the same age (Fig. 7*I*,*J*).

Finally, *in vivo* ERK inhibition by U0126 resulted in a significant improvement in the phenotype and survival of severe SMA-like mice compared with vehicle-treated counterparts. The mean survival increased from 1.66 ± 0.55 d for the vehicle-treated SMA-like mice to 4.73 ± 1.30 d for the U0126-treated mice (Fig. 7*K*), representing a 2.8-fold increase in lifespan ($p < 0.001$). In addition, the U0126 treatment led to a significant and progressive increase in the body weight of SMA-like mice, until death (Fig. 7*L*). Importantly, ERK inhibition significantly improved motor capacities of SMA-like mice as evidenced by the ability of U0126-treated, in contrast to vehicle-treated, SMA-like mice to get back on their feet after being placed on their side (Fig. 7*M*). In addition, the spontaneous activity and the mobility of SMA-like mice significantly increased with U0126 treatment as evidenced by the open-field test (Fig. 7*N*,*O*).

The inhibition of the MEK/ERK/Elk-1 pathway by Selumetinib, a clinically applicable drug, is remarkably beneficial for type 1 SMA-like mice

These results prompted us to test whether a clinically applicable MEK inhibitor could provide the same effects of U0126 on both the SMN expression and the lifespan of type 1 SMA-like mice. We chose to test a new drug, Selumetinib (AZD6244), an MEK inhibitor leading to ERK inhibition, which is currently in Phase II clinical trials (Board et al., 2009), successfully tested in the Pediatric Preclinical Testing program (Kolb et al., 2010). Expectedly, oral Selumetinib treatment ($5\ mg \cdot kg^{-1} \cdot d^{-1}$) mimics the effects of U0126 administration. ERK inhibition by Selumetinib results in a significant enhancement of SMN expression in the

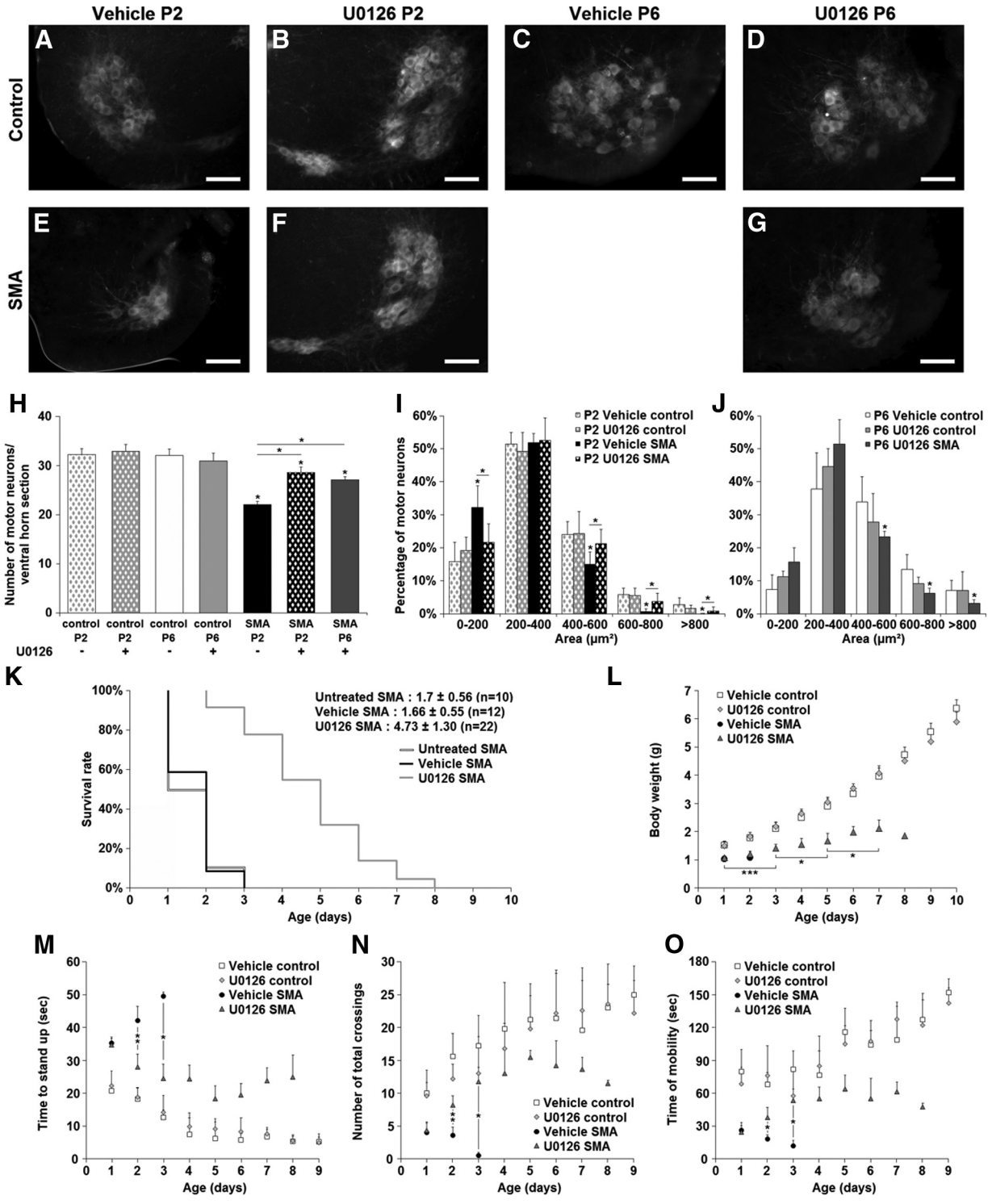

Figure 7. Inhibition of ERK pathway by U0126 induces a significant motor neuron protection, increases lifespan, and improves weight curve in severe SMA-like mice. ***A–G***, Immunodetection of ChAT-positive motor neurons in the lumbar spinal cord (L1–L5) of vehicle-treated (***A***) and U0126-treated control (***B***) mice at 2 d of age, vehicle-treated (***C***) and U0126-treated control (***D***) mice at 6 d of age, vehicle-treated (***E***) and U0126-treated SMA-like mice at 2 d of age (***F***), and U0126-treated SMA-like mice at 6 d of age (***G***). Scale bars, 100 μm. ***H–J***, Quantitative analysis of the number (***H***) and the cell body area (***I***, ***J***) of motor neurons per ventral horn in the ventral lumbar spinal cord of vehicle- and U0126-treated control mice at 2 and 6 d of age, vehicle-treated SMA-like mice at 2 d of age, and vehicle- and U0126-treated SMA-like mice at 6 d of age ($n = 4$). ***K***, Lifespan of U0126-treated SMA-like mice ($n = 22$) compared with vehicle-treated ($n = 12$) and untreated SMA-like mice ($n = 10$). ***L***, Weight curve in U0126-treated ($n = 22$) and vehicle-treated SMA-like mice ($n = 12$) compared with U0126-treated ($n = 15$) and vehicle-treated control ($n = 15$) mice. ***M***, Time spent to stand up after being placed on the side for vehicle-treated ($n = 5$) and U0126-treated control ($n = 5$) mice compared with vehicle-treated ($n = 5$) and U0126-treated SMA-like mice ($n = 5$). ***N***, ***O***, Total number of crossings (***N***) and mobility (***O***) during 5 min in the open-field test for vehicle-treated ($n = 5$) and U0126-treated control ($n = 5$) mice compared with vehicle-treated ($n = 5$) and U0126-treated SMA-like ($n = 5$) mice. Data are displayed as mean ± SEM. *$p < 0.05$, **$p < 0.01$, ***$p < 0.001$.

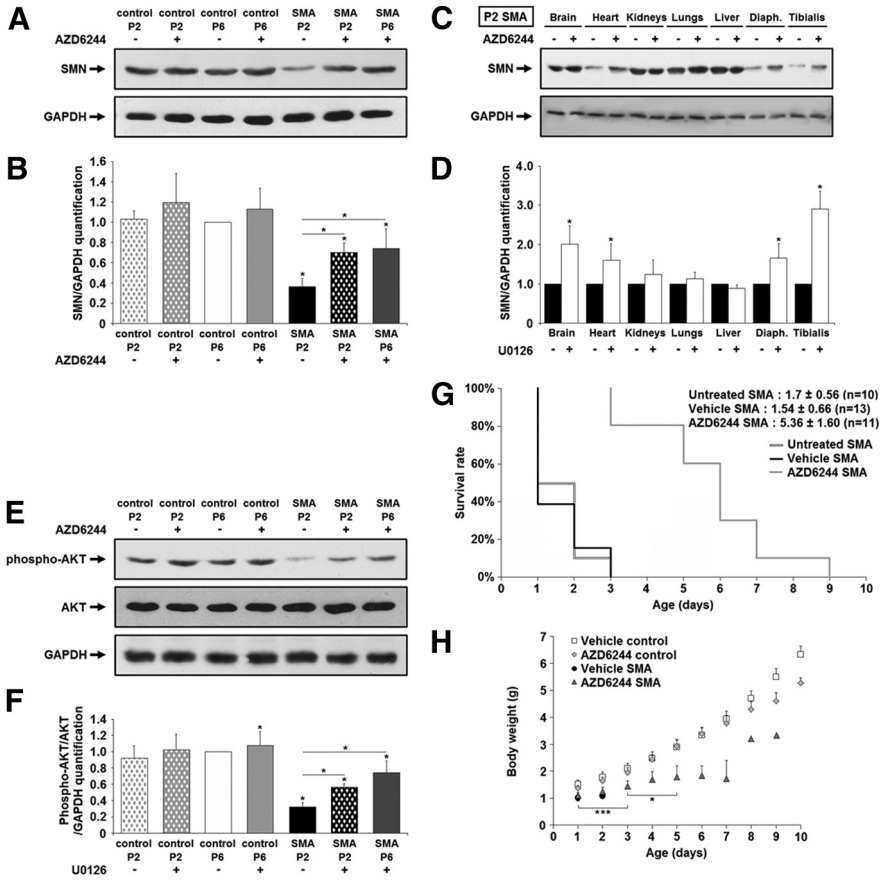

Figure 8. Inhibition of ERK pathway by AZD6244 (Selumetinib) significantly enhances SMN expression and AKT activation, increases lifespan, and improves weight curve in severe SMA-like mice. ***A***, ***B***, Western blot analysis and quantification of SMN protein expression in the ventral lumbar spinal cord of vehicle- and AZD6244-treated control mice at 2 and 6 d of age, vehicle-treated SMA-like mice at 2 d of age, and AZD6244-treated SMA-like mice at 2 and 6 d of age ($n = 3$). ***C***, ***D***, Western blot analysis and quantification of SMN protein expression in brain, heart, kidneys, lungs, liver, diaphragm, and tibialis of AZD6244-treated SMA-like mice at 2 d of age ($n = 3$). ***E***, ***F***, Western blot analysis and quantification of AKT protein phosphorylation in the ventral lumbar spinal cord of vehicle- and AZD6244-treated control mice at 2 and 6 d of age, vehicle-treated SMA-like mice at 2 d of age, and AZD6244-treated SMA-like mice at 2 and 6 d of age ($n = 3$). ***G***, Lifespan of AZD6244-treated SMA-like mice ($n = 11$) compared with vehicle-treated ($n = 13$) and untreated ($n = 10$) SMA-like mice. ***H***, Weight curve in AZD6244-treated ($n = 11$) and vehicle-treated SMA-like ($n = 13$) mice compared with AZD6244-treated ($n = 10$) and vehicle-treated control ($n = 10$) mice. Data are displayed as mean ± SEM. $^{*}p < 0.05$, $^{***}p < 0.001$.

spinal cord of SMA-like mice (Fig. 8*A*,*B*). As found after U0126 treatment, the Selumetinib-induced increase in SMN expression proved to be tissue dependent (Fig. 8*C*,*D*). Furthermore, the treatment resulted in the significant activation of AKT (Fig. 8*E*,*F*).

Most importantly, the Selumetinib treatment significantly increased the survival of type 1 SMA-like mice compared with vehicle-treated SMA-like mice (Fig. 8*G*). The mean survival increased from 1.54 ± 0.66 d for the vehicle-treated mice to 5.36 ± 1.60 d for the Selumetinib-treated mice, representing a 3.4-fold increase in lifespan ($p < 0.001$). Finally, the Selumetinib treatment led to a significant increase in the body weight of type 1 SMA-like mice, until death (Fig. 8*H*).

Discussion

The present study provides the first lines of evidence that the drug inhibition of the MEK/ERK/Elk-1 signaling pathway could be beneficial for severe types of SMA. The ERK inhibition resulted in the activation of the AKT/CREB pathway, leading to a significant increase in the lifespan of type 1 SMA-like mice, treated in the symptomatic phase of the disease. A threefold increase in lifespan was recorded with this treatment, which correlates with a significant neuroprotection in the spinal motor neurons. Importantly, the ERK inhibition induces a marked increase in the concentration of SMN in SMA motor neurons. Furthermore, the role of ERK inhibition on the SMN protein expression has been confirmed in human differentiated muscle cells derived from severe SMA patients.

Although the AKT/CREB pathway is primarily considered as beneficial for neurons, notably in a neurodegenerative context (van der Heide et al., 2006; Lunn et al., 2009; Jimenez et al., 2011), the role of the ERK/Elk-1 pathway in determining the fate of neurons is more contrasted and seems to vary according to the neuronal injury model (Maiese et al., 1993; Ueda et al., 1996; Meyer-Franke et al., 1998; Cha et al., 2000; Colucci-D'Amato et al., 2003; Cheung et al., 2004). Few studies have addressed the role of the ERK pathway in motor neurons in normal or pathological contexts (Hollis et al., 2009). Our present data suggest that, in the specific context of SMA, the ERK/Elk-1 pathway, which is constitutively overactivated in the spinal cord of SMA-like mice (Biondi et al., 2010), exerts a repressive role in *SMN2* gene transcription, therefore likely participating in SMA pathogenesis. Moreover, inhibiting ERK in human SMA myotubes led to a significant increase in SMN, suggesting that the potential repressive role of the ERK/Elk-1 pathway in *SMN2* gene transcription might also occur in humans. These data constitute the first lines of evidence for a repression of *SMN2* gene expression in SMA tissues and contrast with previous observations reporting comparable levels of *SMN2* expression in skin and blood of SMA patients and controls (Also-Rallo et al., 2011). This discrepancy might be attributable to the cell specificity in the pattern of intracellular transduction pathway activity. Although Elk-1 was generally known as a transactivating factor notably through the constitution of the SRF complex (Gille et al., 1995), a repressive role for Elk-1 has been reported previously in some uncommon circumstances (Besnard et al., 2011). Nevertheless, in the spinal cord of type 1 SMA-like mice, the fixation of Elk-1 on its two tested response elements situated in the *SMN2* gene promoter was correlated with site-specific histone deacetylations that encompass neighbor response elements for CREB. CREB is considered as the main transactivating factor for SMN gene transcription (Majumder et al., 2004). Accordingly, inhibiting Elk-1 phosphorylation through MEK/ERK pathway inhibition resulted in the significant increase in acetylation of the two sites, including the CREB response elements. When CREB is activated in SMA spinal cord, as it is the case after ERK inhibition, the binding of CREB to its response elements is significantly increased and correlates with an increase in histone acetylation. In SMA motor neurons, these molecular events at the level of the *SMN2* gene promoter corre-

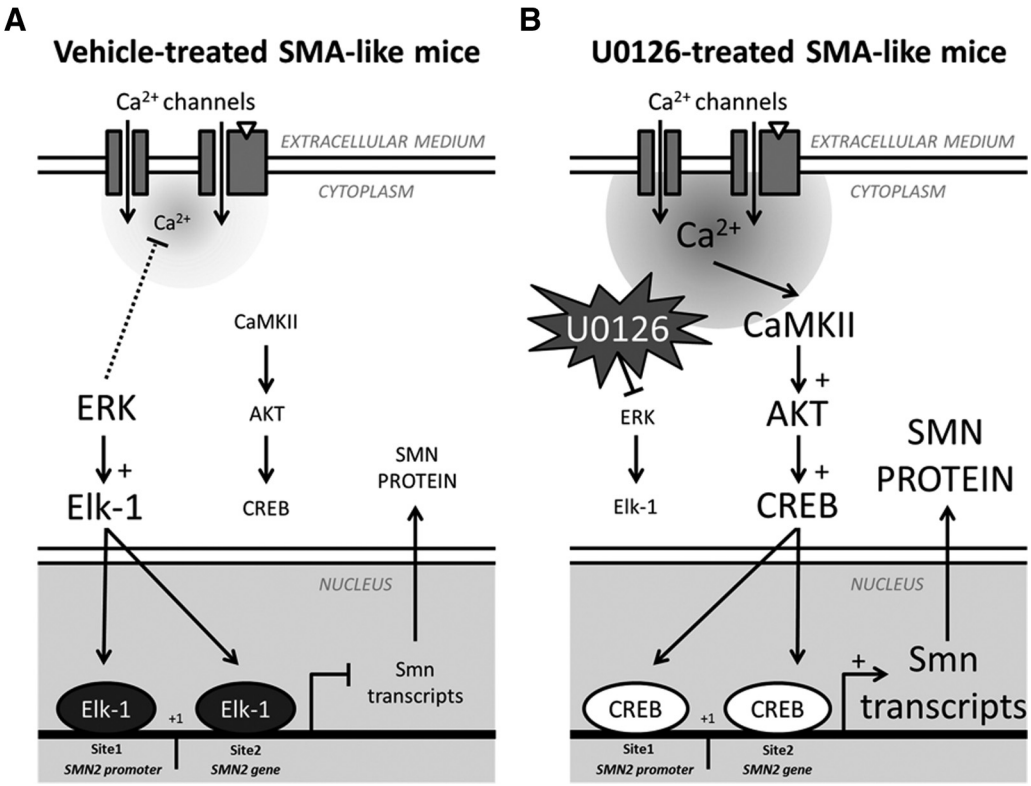

Figure 9. Proposed mechanisms involved in the increase of SMN expression induced by ERK inhibition in the spinal cord of severe SMA-like mice. ***A***, Activation profile of ERK/Elk-1 and AKT/CREB signaling pathways in lumbar spinal cord of vehicle-treated SMA-like mice compared with control. Large characters indicate activated molecules. ***B***, Activation profile of ERK/Elk-1 and AKT/CREB signaling pathways in lumbar spinal cord of U0126-treated SMA-like mice compared with vehicle-treated SMA-like mice. Large characters indicate activated molecules.

lated with a significant increase in SMN expression that is likely to result from *SMN2* gene transcriptional activation. According to this hypothesis, kinetic analyses revealed that ERK inhibition resulted in CREB activation within the hour, leading to a rapid *SMN2* gene activation that can be detected as early as 2 h after ERK inhibition. This cascade of molecular events likely resulted in an acute SMN increase in expression explaining why the SMN level did not progressively increase with treatment. All these data suggest that Elk-1 and CREB compete for the same sites, leading to the recruitment of either a repressive or an activatory transcription complex. Importantly, in human SMA myotubes, ERK inhibition correlated also with a significant increase of SMN expression. In addition to *SMN2* gene transcriptional activation, an increase in SMN transcript stability after ERK inhibition cannot be excluded on the basis of our data. However, the activation of another MAPK, the p38 MAPK, was shown to efficiently stabilize SMN transcripts through RNA binding protein HuR (Farooq et al., 2009).

Unexpectedly, the role of Elk-1 in repressing SMN gene expression proved to be restricted to SMA tissues. Indeed, the Elk-1 deprivation in neuronal cell culture resulted in a significant decrease in SMN expression (Demir et al., 2011), and the present data revealed that, in control spinal cords, ERK inhibition resulted also in an increase in SMN expression independently of Elk-1 activation profile (Figs. 1*A*,*B*, 2*C*,*D*). This discrepancy in ERK inhibition response in control and SMA tissues may result from the likely alteration of a number of signaling pathways in SMA tissues (Millino et al., 2009), among which some might converge to transcription factors such as Elk-1 or CREB.

Moreover, our data suggest the hypothesis of a dynamic equilibrium between the MEK/ERK/Elk-1 and AKT/CREB pathways in SMA spinal and muscle cells that can be shifted by reciprocal blockade. Although ERK and AKT signaling pathways are often simultaneously activated in response to growth factors and hormones (Katz and McCormick, 1997; Rodriguez-Viciana et al., 1997) and are thought to synergize to provide a more robust signal (Rommel et al., 1999; von Gise et al., 2001), putative negative crosstalks among those resulting in the control of neuron survival (Subramanian et al., 2005) or of muscle differentiation (Rommel et al., 1999) have been proposed. In such cases, AKT pathway activation induced ERK pathway inhibition. The present study provides the first line of evidence of an ERK-dependent inhibition of the AKT/CREB pathway in the spinal cord. Using inhibitors at different levels of each signaling cascade, we reported here that the crosstalk between ERK and AKT pathways are sequential and reciprocal in SMA spinal and muscle cells. Furthermore, our data suggested that the signal could shift to a parallel pathway when an intermediary molecule, situated downstream as the transcription factor such as CREB in the AKT pathway, is inhibited. In that case, similar to what has been described for key enzymes of the metabolic pathways, there is first a negative feedback event, the upstream intermediary (e.g., AKT), being deactivated and, second, a shift to a parallel signaling pathway (e.g., ERK) through the activation of an upstream molecule. Accordingly, inhibiting ERK would sequentially result in AKT and CREB activations, thus increasing SMN expression that would ultimately suggest a beneficial use of ERK inhibition for SMA treatment.

Although the mechanisms involved in ERK-dependent inhibition of the AKT pathway require additional investigation, the present data unexpectedly suggest an ERK-dependent inhibition of intracellular calcium influx. Inhibiting ERK rapidly resulted in

an important calcium influx in the cytoplasm of spinal neurons, which share common electrophysiological properties with motor neurons. This ERK-inhibition-induced calcium influx appeared significantly higher in SMA neurons compared with control cells, strengthening the hypothesis of a sustained blockade of the ERK-dependent calcium channels in SMA spinal cord in which ERK is constitutively overactivated (Biondi et al., 2010). This observation could provide additional clues for explaining the reduced frequency of local Ca^{2+} transients observed in cultured (*Smn*)-deficient motor neurons (Jablonka et al., 2007). In addition, the crucial role of the calcium influx in ERK-inhibition-induced intracellular signaling was further evidenced by the effects of the calcium chelation that completely abolished the shift toward the AKT pathway and the consecutive SMN expression increase in SMA spinal cord. The relevant calcium channels, the opening of which is under the control of ERK, have yet to be identified. Nevertheless, the present data led us to speculate that, in the specific context of SMA, the constitutive overactivation of the ERK pathway might participate in the alteration of Ca^{2+} homeostasis, as reported in the nerve terminal of another severe type SMA-like mouse model (Ruiz et al., 2010).

The time course of the ERK to AKT shift strongly suggested that the interconnection between ERK and AKT pathways is unlikely to include an additional transcription step. Furthermore, the molecule responsible for the shift has to be dependent on Ca^{2+} for its activation and situated upstream of ERK and AKT in each signaling pathway. CaMKII, which is directly involved in AKT activation after ERK inhibition (Fig. 4), might be this dual specificity key controlling molecule. CaMKs belong to a well-known calcium-signal-decoding kinase family that is able to transduce the signal from the cell surface to the nucleus through the phosphorylation of some intermediary kinases, such as ERK or AKT, or transcription factors, such as CREB or Elk-1 (Johnson et al., 1997; Lee et al., 2004). The signaling cascades initiated by CaMK activation are likely to occur in a cell-dependent manner (Johnson et al., 1997). Very few studies have been devoted to the signaling pathway that is situated downstream CaMKII in the ventral spinal cord (Wan and Poo, 1999). The present data suggest that, in the spinal motor columns, decoding the calcium signal involves the sequential activation of CaMKII, AKT, and finally CREB. Inhibiting one of the kinases in this pathway would impair the activation of the transcription factor and, ultimately, the increase in *SMN2* gene expression.

Finally, in the light of all these results, it is tempting to speculate that, in SMA motor neurons and myotubes, the low activity of the motor system, associated with the intracellular sustained level of ERK activation, would lower the cytoplasmic concentration of Ca^{2+} and consequently the activation profile of Ca^{2+}-dependent signaling kinases, such as CaMKII and their respective downstream signaling cascades involving AKT and CREB. The fact that, in control spinal cord, chelating intracellular Ca^{2+} by BAPTA-AM induced a significant decrease in SMN expression (Fig. 5), suggests that, even in normal conditions, a threshold intracellular Ca^{2+} concentration is essential for keeping SMN expression at a constant level. Accordingly, inducing an intracellular Ca^{2+} influx in SMA motor neurons or myotubes, through either an increase in neuron activity with physical exercise or more directly through the activation of cell surface calcium channels, such as the NMDA receptor (Biondi et al., 2010), activates CaMKII, resulting in both the activation of AKT and inhibition of ERK. One consequence of the latter signaling event would be the de-inhibition of several hitherto unidentified calcium channels, ultimately leading to synergistic increase in the Ca^{2+} influx (Fig. 9).

Most importantly, all these data strengthen the assumption that the drug inhibition of the ERK pathway would constitute a means of increasing SMN expression in the spinal cord of severe SMA types. Our study used the well-established severe SMA mouse model (Monani et al., 2000) that has been treated in the symptomatic phase of the disease as indicated for humans. Interestingly, analyzing the effects of ERK inhibition in mouse models of milder SMA type will be useful in benchmarking against other known inhibitors. Importantly, we tested the effects of two different ERK inhibitors both administered by intrathecal injections or orally with identical results. Among those, we tested Selumetinib (AZD6244) from Selleck Chemicals. This drug, orally administrated, has little secondary effects and is already in Phase II clinical trials for the treatment of specific cancers (Board et al., 2009). Selumetinib would constitute a bona fide candidate molecule to be tested on symptomatic type 1 SMA patients.

References

Also-Rallo E, Alías L, Martínez-Hernández R, Caselles L, Barceló MJ, Baiget M, Bernal S, Tizzano EF (2011) Treatment of spinal muscular atrophy cells with drugs that upregulate SMN expression reveals inter- and intra-patient variability. Eur J Hum Genet 10:1059–1065. CrossRef Medline

Avila AM, Burnett BG, Taye AA, Gabanella F, Knight MA, Hartenstein P, Cizman Z, Di Prospero NA, Pellizzoni L, Fischbeck KH, Sumner CJ (2007) Trichostatin A increases SMN expression and survival in a mouse model of spinal muscular atrophy. J Clin Invest 117:659–671. CrossRef Medline

Besnard A, Galan-Rodriguez B, Vanhoutte P, Caboche J (2011) Elk-1 a transcription factor with multiple facets in the brain. Front Neurosci 5:35. CrossRef Medline

Bigot A, Klein AF, Gasnier E, Jacquemin V, Ravassard P, Butler-Browne G, Mouly V, Furling D (2009) Large CTG repeats trigger p16-dependent premature senescence in myotonic dystrophy type 1 muscle precursor cells. Am J Pathol 174:1435–1442. CrossRef Medline

Biondi O, Branchu J, Sanchez G, Lancelin C, Deforges S, Lopes P, Pariset C, Lécolle S, Côté J, Chanoine C, Charbonnier F (2010) *In vivo* NMDA receptor activation accelerates motor unit maturation, protects spinal motor neurons, and enhances SMN2 gene expression in severe spinal muscular atrophy mice. J Neurosci 30:11288–11299. CrossRef Medline

Board RE, Ellison G, Orr MC, Kemsley KR, McWalter G, Blockley LY, Dearden SP, Morris C, Ranson M, Cantarini MV, Dive C, Hughes A (2009) Detection of BRAF mutations in the tumour and serum of patients enrolled in the AZD6244 (ARRY-142886) advanced melanoma phase II study. Br J Cancer 101:1724–1730. CrossRef Medline

Butchbach ME, Singh J, Thorsteinsdóttir M, Saieva L, Slominski E, Thurmond J, Andrésson T, Zhang J, Edwards JD, Simard LR, Pellizzoni L, Jarecki J, Burghes AH, Gurney ME (2010) Effects of 2,4-diaminoquinazoline derivatives on SMN expression and phenotype in a mouse model for spinal muscular atrophy. Hum Mol Genet 19:454–467. CrossRef Medline

Cha YK, Kim YH, Ahn YH, Koh JY (2000) Epidermal growth factor induces oxidative neuronal injury in cortical culture. J Neurochem 75:298–303. CrossRef Medline

Chang JG, Hsieh-Li HM, Jong YJ, Wang NM, Tsai CH, Li H (2001) Treatment of spinal muscular atrophy by sodium butyrate. Proc Natl Acad Sci U S A 98:9808–9813. CrossRef Medline

Cheung NS, Koh CH, Bay BH, Qi RZ, Choy MS, Li QT, Wong KP, Whiteman M (2004) Chronic exposure to U18666A induces apoptosis in cultured murine cortical neurons. Biochem Biophys Res Commun 315:408–417. CrossRef Medline

Colucci-D'Amato L, Perrone-Capano C, di Porzio U (2003) Chronic activation of ERK and neurodegenerative diseases. Bioessays 25:1085–1095. CrossRef Medline

Crawford TO, Pardo CA (1996) The neurobiology of childhood spinal muscular atrophy. Neurobiol Dis 3:97–110. CrossRef Medline

Demir O, Aysit N, Onder Z, Turkel N, Ozturk G, Sharrocks AD, Kurnaz IA (2011) ETS-domain transcription factor Elk-1 mediates neuronal survival: SMN as a potential target. Biochim Biophys Acta 1812:652–662. CrossRef Medline

Denton CL, Gustafson DL (2011) Pharmacokinetics and pharmacodynamics of AZD6244 (ARRY-142886) in tumor-bearing nude mice. Cancer Chemother Pharmacol 67:349–360. CrossRef Medline

Farooq F, Balabanian S, Liu X, Holcik M, MacKenzie A (2009) p38 Mitogen-activated protein kinase stabilizes SMN mRNA through RNA binding protein HuR. Hum Mol Genet 18:4035–4045. CrossRef Medline

Gille H, Strahl T, Shaw PE (1995) Activation of ternary complex factor Elk-1 by stress-activated protein kinases. Curr Biol 5:1191–1200. CrossRef Medline

Heier CR, DiDonato CJ (2009) Translational readthrough by the aminoglycoside geneticin (G418) modulates SMN stability in vitro and improves motor function in SMA mice in vivo. Hum Mol Genet 18:1310–1322. CrossRef Medline

Hollis ER 2nd, Jamshidi P, Löw K, Blesch A, Tuszynski MH (2009) Induction of corticospinal regeneration by lentiviral trkB-induced Erk activation. Proc Natl Acad Sci U S A 106:7215–7220. CrossRef Medline

Jablonka S, Beck M, Lechner BD, Mayer C, Sendtner M (2007) Defective Ca^{2+} channel clustering in axon terminals disturbs excitability in motoneurons in spinal muscular atrophy. J Cell Biol 179:139–149. CrossRef Medline

Jimenez S, Torres M, Vizuete M, Sanchez-Varo R, Sanchez-Mejias E, Trujillo-Estrada L, Carmona-Cuenca I, Caballero C, Ruano D, Gutierrez A, Vitorica J (2011) Age-dependent accumulation of soluble amyloid beta (Abeta) oligomers reverses the neuroprotective effect of soluble amyloid precursor protein-alpha (sAPP(alpha)) by modulating phosphatidylinositol 3-kinase (PI3K)/Akt-GSK-3beta pathway in Alzheimer mouse model. J Biol Chem 286:18414–18425. CrossRef Medline

Johnson CM, Hill CS, Chawla S, Treisman R, Bading H (1997) Calcium controls gene expression via three distinct pathways that can function independently of the Ras/mitogen-activated protein kinases (ERKs) signaling cascade. J Neurosci 17:6189–6202. Medline

Katz ME, McCormick F (1997) Signal transduction from multiple Ras effectors. Curr Opin Genet Dev 7:75–79. CrossRef Medline

Kobayashi T, Askanas V, Engel WK (1987) Human muscle cultured in monolayer and cocultured with fetal rat spinal cord: importance of dorsal root ganglia for achieving successful functional innervation. J Neurosci 7:3131–3141. Medline

Kolb EA, Gorlick R, Houghton PJ, Morton CL, Neale G, Keir ST, Carol H, Lock R, Phelps D, Kang MH, Reynolds CP, Maris JM, Billups C, Smith MA (2010) Initial testing (stage 1) of AZD6244 (ARRY-142886) by the Pediatric Preclinical Testing Program. Pediatr Blood Cancer 55:668–677. CrossRef Medline

Lee SJ, Campomanes CR, Sikat PT, Greenfield AT, Allen PB, McEwen BS (2004) Estrogen induces phosphorylation of cyclic AMP response element binding (pCREB) in primary hippocampal cells in a time-dependent manner. Neuroscience 124:549–560. CrossRef Medline

Lefebvre S, Bürglen L, Reboullet S, Clermont O, Burlet P, Viollet L, Benichou B, Cruaud C, Millasseau P, Zeviani M, Le Paslier D, Frézal J, Cohen D, Weissenbach J, Munnich A, Melki J (1995) Identification and characterization of a spinal muscular atrophy-determining gene. Cell 80:155–165. CrossRef Medline

Lorson CL, Androphy EJ (2000) An exonic enhancer is required for inclusion of an essential exon in the SMA-determining gene SMN. Hum Mol Genet 9:259–265. CrossRef Medline

Lorson CL, Rindt H, Shababi M (2010) Spinal muscular atrophy: mechanisms and therapeutic strategies. Hum Mol Genet 19:R111–R118. CrossRef Medline

Lunn JS, Sakowski SA, Kim B, Rosenberg AA, Feldman EL (2009) Vascular endothelial growth factor prevents G93A-SOD1-induced motor neuron degeneration. Dev Neurobiol 69:871–884. CrossRef Medline

Maiese K, Boniece IR, Skurat K, Wagner JA (1993) Protein kinases modulate the sensitivity of hippocampal neurons to nitric oxide toxicity and anoxia. J Neurosci Res 36:77–87. CrossRef Medline

Majumder S, Varadharaj S, Ghoshal K, Monani U, Burghes AH, Jacob ST (2004) Identification of a novel cyclic AMP-response element (CRE-II) and the role of CREB-1 in the cAMP-induced expression of the survival motor neuron (SMN) gene. J Biol Chem 279:14803–14811. CrossRef Medline

Mercuri E, Bertini E, Messina S, Solari A, D'Amico A, Angelozzi C, Battini R, Berardinelli A, Boffi P, Bruno C, Cini C, Colitto F, Kinali M, Minetti C, Mongini T, Morandi L, Neri G, Orcesi S, Pane M, Pelliccioni M, et al. (2007) Randomized, double-blind, placebo-controlled trial of phenylbutyrate in spinal muscular atrophy. Neurology 68:51–55. CrossRef Medline

Meyer-Franke A, Wilkinson GA, Kruttgen A, Hu M, Munro E, Hanson MG Jr, Reichardt LF, Barres BA (1998) Depolarization and cAMP elevation rapidly recruit TrkB to the plasma membrane of CNS neurons. Neuron 21:681–693. CrossRef Medline

Millino C, Fanin M, Vettori A, Laveder P, Mostacciuolo ML, Angelini C, Lanfranchi G (2009) Different atrophy-hypertrophy transcription pathways in muscles affected by severe and mild spinal muscular atrophy. BMC Med 7:14. CrossRef Medline

Monani UR, Sendtner M, Coovert DD, Parsons DW, Andreassi C, Le TT, Jablonka S, Schrank B, Rossoll W, Prior TW, Morris GE, Burghes AH (2000) The human centromeric survival motor neuron gene (SMN2) rescues embryonic lethality in Smn(−/−) mice and results in a mouse with spinal muscular atrophy. Hum Mol Genet 9:333–339. CrossRef Medline

Rodriguez-Viciana P, Warne PH, Khwaja A, Marte BM, Pappin D, Das P, Waterfield MD, Ridley A, Downward J (1997) Role of phosphoinositide 3-OH kinase in cell transformation and control of the actin cytoskeleton by Ras. Cell 89:457–467. CrossRef Medline

Rommel C, Clarke BA, Zimmermann S, Nuñez L, Rossman R, Reid K, Moelling K, Yancopoulos GD, Glass DJ (1999) Differentiation stage-specific inhibition of the Raf-MEK-ERK pathway by Akt. Science 286:1738–1741. CrossRef Medline

Ruiz R, Casañas JJ, Torres-Benito L, Cano R, Tabares L (2010) Altered intracellular Ca^{2+} homeostasis in nerve terminals of severe spinal muscular atrophy mice. J Neurosci 30:849–857. CrossRef Medline

Subramanian C, Opipari AW Jr, Castle VP, Kwok RP (2005) Histone deacetylase inhibition induces apoptosis in neuroblastoma. Cell Cycle 4:1741–1743. CrossRef Medline

Sutton G, Chandler LJ (2002) Activity-dependent NMDA receptor-mediated activation of protein kinase B/Akt in cortical neuronal cultures. J Neurochem 82:1097–1105. CrossRef Medline

Swoboda KJ, Scott CB, Reyna SP, Prior TW, LaSalle B, Sorenson SL, Wood J, Acsadi G, Crawford TO, Kissel JT, Krosschell KJ, D'Anjou G, Bromberg MB, Schroth MK, Chan GM, Elsheikh B, Simard LR (2009) Phase II open label study of valproic acid in spinal muscular atrophy. PLoS One 4:e5268. CrossRef Medline

Swoboda KJ, Scott CB, Crawford TO, Simard LR, Reyna SP, Krosschell KJ, Acsadi G, Elsheik B, Schroth MK, D'Anjou G, LaSalle B, Prior TW, Sorenson SL, Maczulski JA, Bromberg MB, Chan GM, Kissel JT; Project Cure Spinal Muscular Atrophy Investigators Network (2010) SMA CARNI-VAL trial part I: double-blind, randomized, placebo-controlled trial of L-carnitine and valproic acid in spinal muscular atrophy. PLoS One 5:e12140. CrossRef Medline

Thurmond J, Butchbach ME, Palomo M, Pease B, Rao M, Bedell L, Keyvan M, Pai G, Mishra R, Haraldsson M, Andresson T, Bragason G, Thosteinsdottir M, Bjornsson JM, Coovert DD, Burghes AH, Gurney ME, Singh J (2008) Synthesis and biological evaluation of novel 2,4-diaminoquinazoline derivatives as SMN2 promoter activators for the potential treatment of spinal muscular atrophy. J Med Chem 51:449–469. CrossRef Medline

Towbin H, Schoenenberger C, Ball R, Braun DG, Rosenfelder G (1984) Glycosphingolipid-blotting: an immunological detection procedure after separation by thin layer chromatography. J Immunol Methods 72:471–479. CrossRef Medline

Tsai LK, Tsai MS, Ting CH, Li H (2008) Multiple therapeutic effects of valproic acid in spinal muscular atrophy model mice. J Mol Med (Berl) 86:1243–1254. CrossRef Medline

Ueda K, Yagami T, Kageyama H, Kawasaki K (1996) Protein kinase inhibitor attenuates apoptotic cell death induced by amyloid beta protein in culture of the rat cerebral cortex. Neurosci Lett 203:175–178. CrossRef Medline

van der Heide LP, Ramakers GM, Smidt MP (2006) Insulin signaling in the central nervous system: learning to survive. Prog Neurobiol 79:205–221. CrossRef Medline

von Gise A, Lorenz P, Wellbrock C, Hemmings B, Berberich-Siebelt F, Rapp UR, Troppmair J (2001) Apoptosis suppression by Raf-1 and MEK1 requires MEK- and phosphatidylinositol 3-kinase-dependent signals. Mol Cell Biol 21:2324–2336. CrossRef Medline

Wan J, Poo M (1999) Activity-induced potentiation of developing neuromuscular synapses. Science 285:1725–1728. CrossRef Medline

Whitmarsh AJ, Shore P, Sharrocks AD, Davis RJ (1995) Integration of MAP

kinase signal transduction pathways at the serum response element. Science 269:403–407. CrossRef Medline

Yang SH, Shore P, Willingham N, Lakey JH, Sharrocks AD (1999) The mechanism of phosphorylation-inducible activation of the ETS-domain transcription factor Elk-1. EMBO J 18:5666–5674. CrossRef Medline

Zhang HM, Li L, Papadopoulou N, Hodgson G, Evans E, Galbraith M, Dear M, Vougier S, Saxton J, Shaw PE (2008) Mitogen-induced recruitment of ERK and MSK to SRE promoter complexes by ternary complex factor Elk-1. Nucleic Acids Res 36:2594–2607. CrossRef Medline

Zimmermann S, Moelling K (1999) Phosphorylation and regulation of Raf by Akt (protein kinase B). Science 286:1741–1744. CrossRef Medline